simultaneously in most cancer cell lines, this ligand and receptor are produced in the same secretory pathway. Therefore, this is a good model to investigate the regulatory mechanism of protein production in an autocrine secretory pathway. Here, we developed a new method, ER trapping, which simultaneously suppressed MK secretion and LRP1 maturation. Utilizing this and other techniques, we found that MK interacted with LRP1 not only on the cell surface but also in the secretory pathway during their biosyntheses. We named the latter interaction the premature ligand-receptor interaction. We found that the premature ligand-receptor interaction plays a negative regulatory role in the production of MK and LRP1 within the secretory pathway. Avoiding this premature interaction may allow cancer cells to overproduce a growth factor and may be a strategy of those cells for survival and expansion.

EXPERIMENTAL PROCEDURES

Cells, DNA Constructs, and Antibodies—CHO K1 cells were cultured in DMEM with 10% fetal bovine serum. TGW cells (a human neuroblastoma cell line) were cultured in RPMI 1640 medium with 10% fetal bovine serum. CHO-mini-LRP (mLRP)-I, -mLRP-II, -mLRP-III, -mLRP-IV, and -mLRP-IVm cells and a series of mLRP expression vectors were generated as described previously (23–25). The expression vector for mouse RAP tagged with the FLAG epitope at the C terminus was constructed in pIRES-EGFP (Clontech). The expression vector for human MK was constructed in pcDNA3.1 (Invitrogen). To generate an ER expression vector (ER-TRAP) for a peptide that contained SLRP2N-EGF (25) and the ER retention signal HNEL, the cDNA encoding this peptide was placed underneath the cytomegalovirus promoter of pcDNA3 (Invitrogen). Anti-HA and -FLAG antibodies were purchased from Roche Applied Science and Sigma, respectively. Anti-calnexin and anti-phosphotyrosine (Tyr(P)-100) antibodies were from Stressgen and Cell Signaling, respectively.

Chemical Cross-linking—Radioiodination of MK was performed as described previously (22). The specific activity obtained was $\sim 5 \times 10^7$ cpm/μg. For chemical cross-linking, cells were washed with ice-cold phosphate-buffered saline containing calcium and magnesium (PBS+) as well as 0.1% bovine serum albumin (PBS-BSA), and supplied with 5 ml of ice-cold DMEM with 10% fetal bovine serum. Cells were then incubated with ^{125}I-labeled MK (2×10^7 cpm) at 4 °C for 2 h by gentle rotation. After washing with PBS-BSA three times and PBS+ once, 5 ml of PBS+ was added. The cross-linking was begun by adding the water-soluble (BS3; Pierce) or -insoluble (DSS; Pierce) cross-linker at a final concentration of 0.27 mM and incubating at 4 °C for 15 min. The reaction was stopped with detaching buffer (10 mM Tris-HCl (pH 7.5), 10% glycerol, 1 mM calcium chloride, 1 mM magnesium chloride, and 1 mM PMSF). Cells were scraped in 500 μl of detaching buffer, collected by centrifuge, and lysed with 200 μl of lysis buffer (20 mM Tris-HCl (pH 7.5), 0.6% CHAPS, 150 mM sodium chloride, 1 mM calcium chloride, 1 mM magnesium chloride, and 1 mM PMSF). For *in vitro* cross-linking, 10 μl of protein solution dialyzed against appropriate buffers was mixed with 2 μl of ^{125}I-labeled MK (~10 ng) and was incubated at 20 °C for 1 h. Cross-linking was started by adding 0.2 μl of 20 mM DSS or BS3 and incubating at 4 °C for 10 min. The reaction was stopped by adding 1 μl of 1 M Tris-HCl (pH 7.4) and 4.5 μl of Laemmli 4 × sample buffer.

Sucrose Gradient Analysis—Cells grown in a 10-cm dish were lysed with 0.5 ml of 1% Triton in PBS+ and centrifuged at 15,000 × *g* at 4 °C for 10 min. The supernatant (0.3 ml) was layered on a stepwise sucrose gradient (60% 0.5 ml, 25% 1 ml, 20% 1 ml, 10% 1 ml, and 5% 1 ml in 0.1% Triton in PBS+) in a centrifuge tube (326819 tube; Beckman) and centrifuged at 130,000 × *g* at 17 °C for 19 h (SW50.1 rotor; Beckman). Fractionation was performed by collecting 7 drops/fraction from the bottom of the tube.

Sequential Immunoprecipitation—After the first immunoprecipitation, the immunoprecipitates were suspended in 100 μl of 1% SDS in the lysis buffer, boiled for 3 min, and diluted with 1 ml of the lysis buffer. This solution was then subjected to the second immunoprecipitation.

Generation and Purification of MK-TRAP-Fc—The expression vector for MK-TRAP-Fc was generated in pFUSE-Fc (Invivogen) and transfected into HEK293T cells. After 5 days, the conditioned media were collected and centrifuged to remove cellular debris. A 24-ml aliquot of the supernatants was loaded onto protein G-Sepharose (GE Healthcare) and washed with 30 ml of 20 mM phosphate buffer (pH 7.0). The bound fraction was eluted with 3.6 ml of 100 mM glycine HCl (pH 3.0) and neutralized immediately with 0.4 ml of 1.5 M Tris-HCl (pH 8.8). The purified protein was desalted with PD-10 (GE Healthcare) and concentrated using an Amicon Ultra-4 device (MWCO 3000; Millipore).

In Vitro Binding Assay of MK and MK-TRAP—A 100-μl aliquot of MK-TRAP-Fc solution was immobilized on a 96-well assay plate by incubating overnight at 4 °C. The wells were washed three times with PBS, and varying concentrations of AP-MK were applied. After 90 min at room temperature, unbound AP-MK was washed out by washing five times with HBHA buffer (20 mM HEPES, 0.1% BSA in Hanks' balanced salt solution). Bound AP-MK was estimated by enzymatic assay using *p*-nitrophenylphosphate as a substrate.

Sample Collection of Human Colorectal Carcinoma Tissues—The procedures and sources of sample collection under informed consent were as described previously (26).

Quantitative Real-time RT-PCR—Total RNA was isolated from colorectal tissues with ISOGEN (Nippon Gene). cDNA was obtained using a SuperScript III cDNA synthesis kit (Invitrogen). Quantitative real-time RT-PCR was performed with a TaqMan probe and ABI PRISM 7700 (Applied Biosystems) according to the manufacturer's instructions.

Cell Migration Assay—Chemotaxicells (8-μm pore; Kurabo, Osaka, Japan) were coated, unless otherwise indicated, on the underside surface with 1 μg/ml collagen I in PBS at 37 °C for 1 h. Harvested cells were washed with 10% FBS/DMEM once and 0.4% FBS/DMEM once, then suspended at 4×10^5 cells/ml in 0.4% FBS/DMEM. Collagen I-coated chambers were inserted into wells of a 24-well plate, where each well contained 600 μl of 0.2% BSA and 0.4% FBS/DMEM with or without 50 ng/ml PDGF-BB, and preincubated at room temperature for 10 min. Cells (100 μl) were added to each insert and incubated for 4 h in a CO_2 incubator. Migrating cells were counted at 200 × magnification for five fields/chamber. Experiments were performed

Downloaded from www.jbc.org at NAGOYA UNIV CENTRAL LIBRARY, on March 6, 2012

in triplicate or quadruplicate for each condition, with the numbers of migrating cells being presented as the average ± S.E.

Cell Survival Assay—SW620 cells were transfected with siRNA (siGENOME; Dharmacon) using Lipofectamine 2000 (Invitrogen). After 24 h, cells were seeded onto 96-well plates, and then the medium was switched to 0.5% FBS/F12-K. Viable cells were estimated with a Cell Counting Kit-8 (DOJINDO).

RESULTS

MK Binds to the Second and Fourth Ligand-binding Domains of LRP1 on the Cell Surface—LRP1 consists of two heterodimeric subunits that are produced through furin-mediated processing in the trans-Golgi (Fig. 1*A*). The larger chain (α chain) is extracellular and contains four ligand-binding domains (clusters of ligand-binding repeats). The shorter chain (β chain) contains the transmembrane domain and the cytoplasmic tail. LRP1 was previously identified as a protein bound to the MK-affinity column (21). To clarify the physical association between these two molecules on the cell surface, here we used several membrane-bound mLRP constructs (Fig. 1*A*) (23, 24). The difference between mLRP-IV and mLRP-IVm is that the latter contains a mutation in the intracellular domain. Each mLRP protein carries an HA tag near its N terminus. Each construct was transfected into LRP1-deficient CHO cells. Cells were then incubated with ^{125}I-labeled MK and treated with a water-insoluble chemical cross-linker, DSS.

As shown in Fig. 1*B*, a discrete cross-linked band appeared in wild-type CHO cells (K1) but not in LRP1-deficient CHO cells (LRP1$^{-/-}$). Notably, mLRP-II, -IV, and -IVm-expressing cells showed two cross-linked bands. The upper one represents the unprocessed protein that contains both α and β chains, whereas the lower band is the processed α chain. Because a small fraction of the unprocessed protein is localized on the cell surface,[3] the cross-linked pattern shown in Fig. 1*B* suggests that MK binds to the cell surface α chain containing either the second or fourth ligand-binding domains. Immunoprecipitation with anti-HA antibody confirmed that the cross-linked bands indeed contained the HA-tagged α chain of each mLRP (Fig. 1*C*). A water-soluble cross-linker, BS3, showed the same results (data not shown). Therefore, these data collectively suggest that MK specifically binds to cell surface LRP1.

These data were also consistent with our previous finding in experiments using soluble LRP1 fragments: the N-terminal halves of the second and fourth ligand-binding domains in the LRP1 moiety show the highest affinity to MK (27). We further performed Scatchard plot analysis to reveal the affinity between MK and the N-terminal half of the second ligand-binding domain of LRP1 (formerly designated MK-TRAP; Fig. 1*A*). Indeed, MK and MK-TRAP showed a high affinity with a K_d value of 2.7 nM (Fig. 1, *D* and *E*).

LRP1 Is Required for Intracellular Retention of MK—We next investigated the role of LRP1 in MK production in the secretory pathway by comparing LRP1-deficient and mLRP-IV-expressing cells. In mLRP-IV-expressing cells, co-expression of MK and the LRP1 chaperone RAP enhanced MK secretion into the medium compared with MK expression alone (Fig. 2*A*, *lanes 5* and *6*, *Medium*, *MK*). In contrast, the effect of RAP on MK secretion was not seen in LRP1-deficient cells (LRP1$^{-/-}$) (Fig. 2*A*, *lanes 2* and *3*, *Medium*, *MK*). MK retention in the cell appeared to be reduced by co-expression with RAP (Fig. 2*A*, *lanes 5* and 6, *Cells*, *MK*). Furthermore, translocation of mLRP-IV to the cell surface of MK-expressing cells was significantly reduced compared with that in vector-transfected cells (Fig. 2*A*, *lanes 7* and *8*). This phenomenon was also restored by co-expression of RAP (Fig. 2*A*, *lanes 8* and *9*).

When MK was co-expressed with GFP in mLRP-IV-expressing cells, the intracellular MK was densely stained in nearly detaching, round-shaped cells (Fig. 2*B*, *top row*, *arrowhead*), whereas MK staining became faint by RAP expression (Fig. 2*B*, *middle row*, *arrowheads*). Intracellular localization of MK overlapped that of mLRP-IV (Fig. 2*B*, *bottom row*). Together, these results suggest that LRP1 is essential for intracellular retention of MK during biosynthesis: this retention is probably due to intracellular interaction between MK and LRP1.

Because MK was originally discovered as a retinoic acid-responsive gene product (2), we next investigated endogenous MK protein production using this reagent. Retinoic acid induced MK mRNA expression and consequently intracellular MK protein production in TGW cells, a neuroblastoma cell line (Fig. 2*C*, *RNA* and *Cell*). However, surprisingly, it did not enhance MK protein secretion (Fig. 2*C*, *Medium*). After retinoic acid treatment, LRP1 was detected not only on the cell surface (Fig. 2*D*, *arrows*), but also as a densely stained intracellular body in nearly detaching, round-shaped cells (Fig. 2*D*, *arrowheads*). MK was similarly stained in round cells (Fig. 2*D*), with a pattern reminiscent of MK staining in CHO-mLRP-IV cells (Fig. 2*B*). The detaching, round-shaped cells were thought to be in a state of anoikis, cell death triggered by detachment from the matrix (28). We then tested the effect of RAP on retinoic acid-induced cell death. This chaperone was expected to relieve the ligand-receptor aggregation, based on the results of Fig. 2, *A* and *B*. Indeed, RAP overexpression significantly reduced cell death (Fig. 2*E*).

MK Interacts with Immature LRP1 and Forms Aggregates during Biosynthesis—We next examined the effect of MK expression on LRP1 maturation. Pulse-chase metabolic labeling revealed that the unprocessed (immature) mLRP-IV appeared first (Fig. 3*A*, *open arrow*), and then the processed (mature) mLRP-IV (α and β chains) increased after 60–90-min chase (Fig. 3*A*, *lanes 1–3*, *asterisks*). This profile indicates that the furin-mediated cleavage of immature LRP1 gives rise to mature LRP1, which is consequently presented on the cell surface. A forced expression of MK strongly suppressed LRP1 maturation (Fig. 3*A*, *lanes 4–6*). However, if RAP was co-expressed with MK, LRP1 maturation was restored (Fig. 3*A*, *lanes 7–12*).

It is known that LRP1 aggregates are formed via intermolecular disulfide bonds and appear at the top of the separation gel under nonreducing conditions (29). In the present study, the aggregates increased in cells expressing MK alone but decreased in cells co-expressing MK and RAP (Fig. 3*A*, *Nonreducing*). Taken together, these data suggest that the intracellular MK-LRP1 interaction affects LRP1 maturation.

We next addressed the question of whether or not both MK and LRP1 were involved in aggregate formation. In a sucrose

[3] G. Bu, unpublished data.

Downloaded from www.jbc.org at NAGOYA UNIV CENTRAL LIBRARY, on March 6, 2012

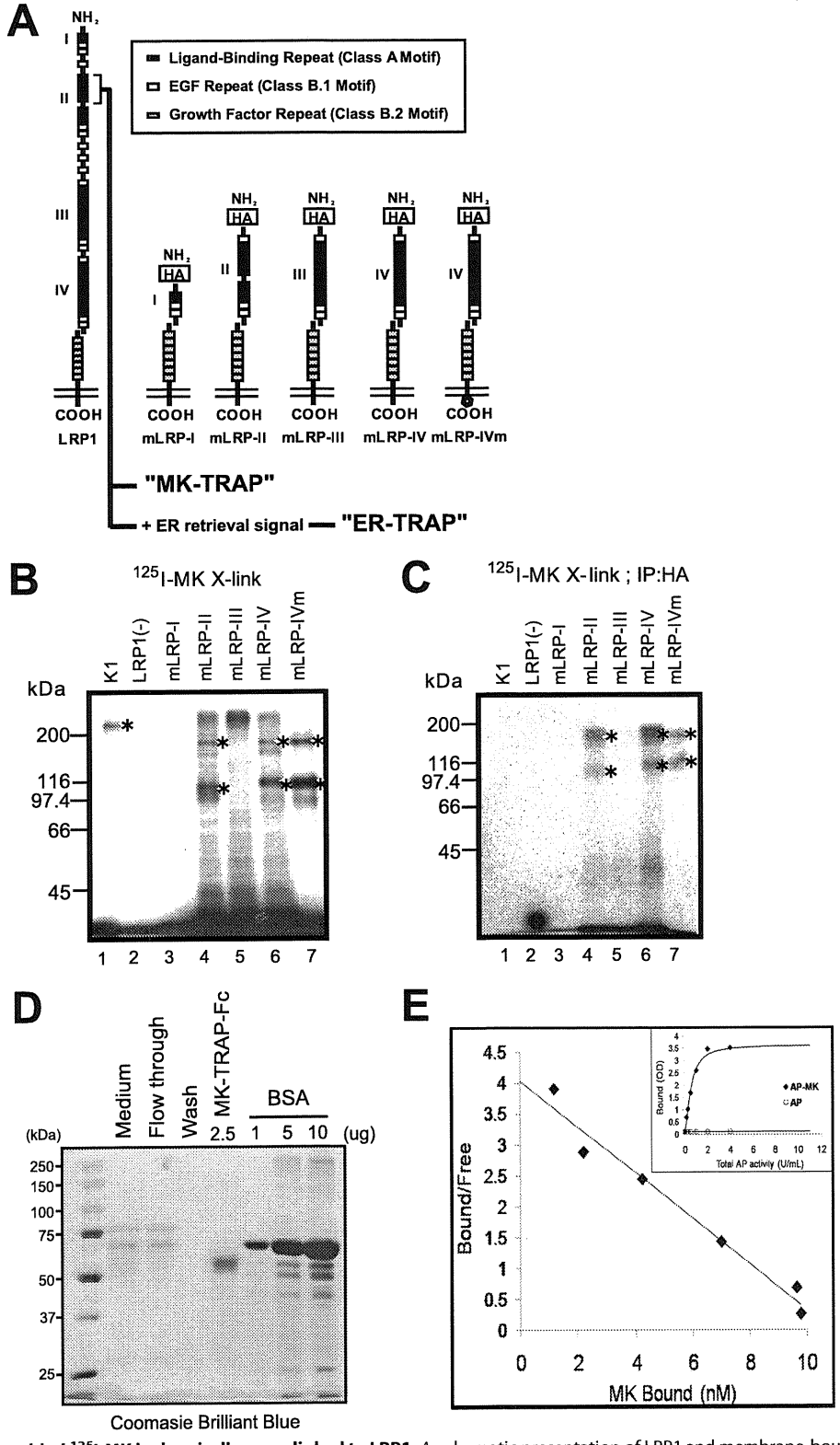

FIGURE 1. **Exogenously added ^{125}I-MK is chemically cross-linked to LRP1.** *A*, schematic presentation of LRP1 and membrane-bound mini-LRP-I, -II, -III, -IV, and -IVmutant. mLRP-IVm has an intracellular domain mutation within its endocytosis signal, which results in cell surface accumulation of this mutant receptor. Biotinylated cell surface mLRP-IV was detected by anti-HA antibody after a pulldown assay with streptavidin-agarose. *B* and *C*, CHO cells cross-linked with ^{125}I-MK (*B*) and immunoprecipitated with anti-HA antibody (*C*). K1 is the wild-type CHO cell line expressing endogenous LRP1. LRP1(−) is a mutant cell line deficient in LRP1. LRP-I, -II, -III, -IV, and -IVm are stable transfectants expressing these genes in the background of LRP1(−) cells. *Asterisks* indicate bands corresponding to various forms of LRP1 (see "Results"). *D*, purified MK-TRAP-Fc subjected to SDS-PAGE and stained with Coomassie Brilliant Blue. *E*, binding kinetics of MK and MK-TRAP-Fc. Scatchard plot analysis yielded a K_d value of 2.7 nM.

Downloaded from www.jbc.org at NAGOYA UNIV CENTRAL LIBRARY, on March 6, 2012

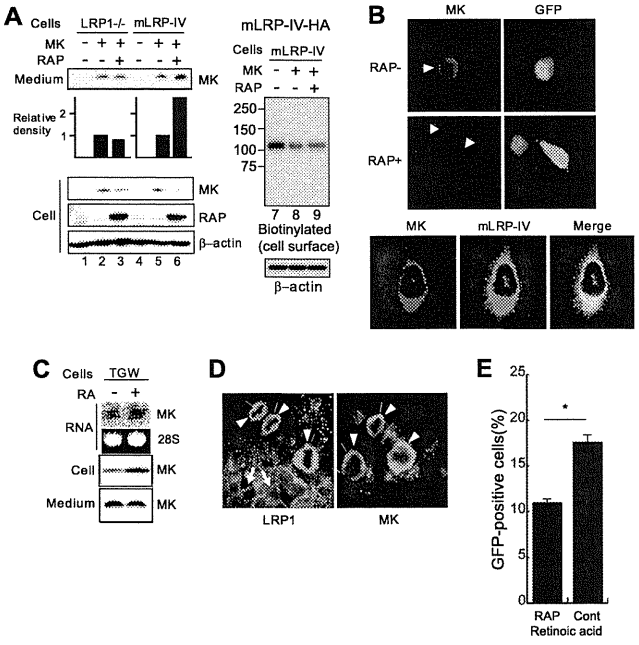

FIGURE 2. **RAP enhances MK secretion.** *A*, CHO LRP1$^{-/-}$ or CHO-mLRP-IV cells were transfected with a combination of MK, RAP, or control vector (−). Results of Western blot analyses are shown. Graphs represent the relative density of each MK band appearing in the *Medium*. *B*, CHO-mLRP-IV cells were transfected with MK and IRES-EGFP (*RAP*−) or MK and RAP-IRES-EGFP (*RAP*+) and then stained with anti-MK antibody. *Arrows* indicate transfected cells. In the *bottom row*, CHO-mLRP-IV cells were transfected with MK-vector. *C*, TGW cells, a human neuroblastoma cell line, were treated with 10^{-6} M retinoic acid for 24 h. RNA and protein expressions were examined by Northern and Western blot analyses, respectively. *D*, LRP1 and MK localization in TGW cells treated with 10^{-6} M retinoic acid is shown. *E*, TGW cells were co-transfected with GFP- and RAP- or control vector and then treated with 10^{-6} M retinoic acid for 48 h. The population of GFP-expressing cells, which represented RAP- or control vector-transfected cells, among detached (dying) cells was determined by FACS. The expression efficiency as estimated on the day after transfection was comparable (~17%) between the RAP and control vectors. *, $p = 0.015$ (Student's *t* test).

density gradient segregation of cellular proteins, bands at the top of the separation gel and smears underneath were detected in void fractions that contained higher molecular mass proteins under a nonreducing condition (Fig. 3*B*, *fractions 1–5*). It has previously been shown that the unprocessed and processed mLRP-IV bands migrate separately under a nonreducing condition (29), and in the present study these bands were detected in fractions 5–11 (*open arrow* and *asterisk*, respectively). MK was detected in the first fraction in addition to the later fractions under the reducing condition, suggesting that MK was also a component of the aggregates (Fig. 3*B*).

To examine the MK-LRP association, we performed immunoprecipitation (*IP*). When pulse-chase-labeled proteins were precipitated with anti-HA antibody (namely, mLRP-IV was precipitated), the unprocessed and processed mLRP-IV were detected at the 90-min chase (*open arrow* and *asterisks*, respectively in Fig. 3*C*, *lane 6*). In contrast, anti-MK antibody co-precipitated the unprocessed mLRP-IV but not the processed one at the 90-min chase (Fig. 3*C*, *lane 2*). Importantly, when RAP was co-expressed with MK, the MK-mLRP association was strongly suppressed (Fig. 3*C*, *lanes 3* and *4*). Fig. 3, *B* and *C*, suggests that MK and immature LRP1 formed a complex during biosynthesis.

To confirm the MK-immature LRP association further, pulse-chase-labeled proteins were sequentially immunoprecipitated by two different antibodies. Fig. 3*D* shows that RAP formed a complex with immature mLRP-IV but not mature mLRP-IV (Fig. 3*D*, *lane 2*). Similarly, the general ER chaperone calnexin as well as MK alone was associated with immature mLRP-IV (Fig. 3*D*, *lanes 3* and *4*).

ER-resident LRP1 Fragment Suppresses MK Secretion and LRP1 Maturation—As shown in Fig. 1*E*, the N-terminal half of the second ligand-binding domain of LRP1 (MK-TRAP) has a high affinity for MK. MK-TRAP traps extracellular MK, blocks MK binding to cell surface LRP1, and consequently suppresses MK function (27). We next utilized this fragment to investigate the biological role of the immature ligand-receptor interaction during biosynthesis. To this end, MK-TRAP was connected with an ER-retrieval signal found in RAP (the amino acid sequence is HNEL), so that MK-TRAP was retained in the ER. We named this construct ER-TRAP (Fig. 1*A*). Because RAP also shows high affinity for the LRP fragment corresponding to MK-TRAP (25), ER-TRAP was expected to trap both MK and RAP in the ER, leading to the suppression of MK secretion and LRP1 maturation.

As shown in Fig. 4*A*, MK-TRAP could be detected in both the cell and the medium, whereas ER-TRAP was only detected in the cell, indicating that ER-TRAP was properly produced as expected. Immunoprecipitation revealed that ER-TRAP bound to both MK and RAP (Fig. 4*B*). ER-TRAP almost completely trapped MK in the cell, leading to cessation of MK secretion, whereas RAP reversed this phenomenon (Fig. 4*C*). ER-TRAP also significantly suppressed endogenous MK secretion in the osteosarcoma cell line, UMR106 (data not shown).

We next examined the effect of ER-TRAP on endogenous LRP1 production. NIH3T3 cells are known to express endogenous LRP1 but not MK. ER-TRAP strongly suppressed the cell surface LRP1 production, as estimated by immunoprecipitation after cell surface biotinylation (Fig. 4*D*). To evaluate the biological significance of this phenomenon, we next examined PDGF-mediated migration because LRP1 is known to suppress PDGF receptor β function, as revealed by a study in which vascular smooth muscle cell-specific knock-out of LRP1 induced increased phosphorylation of PDGF receptor β and enhanced atherosclerosis (30). Although PDGF-BB did not significantly induce migration of NIH3T3 cells when administered alone, it did so in the presence of coated collagen I (Fig. 4*E*). ER-TRAP-transfected cells showed significantly enhanced migration compared with vector-transfected cells, whereas no difference was observed in collagen I-mediated migration (Fig. 4*E*). Moreover, PDGF receptor β phosphorylation in response to exogenous PDGF-BB was induced to a larger extent in ER-TRAP-transfected cells compared with vector-transfected cells (Fig. 4*F*). These results suggest that reduction of cell surface LRP1 reverses LRP1-mediated suppression of PDGF receptor β function.

Increased RAP Expression Is Closely Associated with MK Expression in Human Colorectal Carcinomas—Human carcinomas frequently overproduce MK, and serum MK levels are elevated in cancer patients (9, 10, 13, 26). Based on our findings, we hypothesized that a mechanism preventing MK-LRP1 intra-

Downloaded from www.jbc.org at NAGOYA UNIV CENTRAL LIBRARY, on March 6, 2012

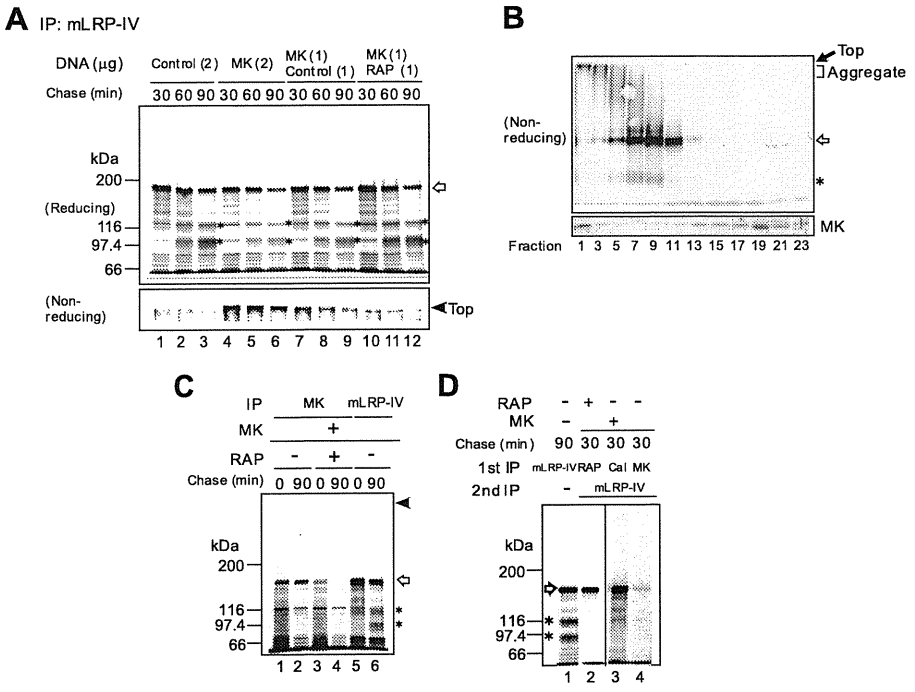

FIGURE 3. **MK binds to unprocessed LRP1 during biosynthesis.** *A*, CHO-mLRP-IV cells were co-transfected with MK- and RAP-vector or control vector (−). Pulse-chase-labeled proteins were immunoprecipitated with an anti-HA antibody that detects mLRP-IV. *Open arrow*, unprocessed mLRP-IV; *asterisks*, processed mLRP-IV. *B*, sucrose gradient analysis was performed for CHO-mLRP-IV cells transfected with an MK-vector as described under "Experimental Procedures." Western blot analysis was performed using anti-HA (*upper panel*, mLRP-IV) or anti-MK antibody (*lower panel*). The *open arrow* and *asterisk* indicate unprocessed and processed mLRP-IV, respectively. *C*, CHO-mLRP-IV cells were transfected with expression vectors as indicated. Immunoprecipitation was performed with anti-MK or anti-HA antibody. *Open arrow*, unprocessed mLRP-IV; *asterisks*, processed mLRP-IV. *D*, CHO-mLRP-IV cells were transfected with expression vectors as indicated. Pulse-chase labeling was performed, and then a sequential immunoprecipitation was performed with the indicated antibodies. *Open arrow*, unprocessed mLRP-IV; *asterisks*, processed mLRP-IV.

cellular aggregation is involved in carcinogenesis. We examined the protein expression of MK and RAP in human colorectal carcinomas and corresponding adjacent normal tissues. In most of the cases examined (33 of 39), MK and RAP were strongly expressed in carcinoma tissues (Fig. 5, *A left*, and *B*). As controls for MK (a ligand of LRP1) and RAP (an ER chaperone), apolipoprotein E (apoE) and calnexin, respectively, were also examined. These control molecules did not show any difference of expression between carcinoma and adjacent normal tissues (Fig. 5*A*, *left*). Real-time RT-PCR examination of the mRNA expression of LRP1 in carcinoma tissues revealed that there were few cases in which the LRP1 expression was reduced compared with the adjacent normal tissue. Thus, among the 20 cases examined, there were 12 cases of up-regulation, 6 cases of no change, and 2 cases of down-regulation (the data of 5 cases corresponding to those in Fig. 5 *left* are shown in Fig. 5 *right*). These results indicate that the MK-LRP1 autocrine loop was activated, and the enhanced expressions of RAP and MK are closely associated in human colorectal carcinomas. To confirm the idea that RAP plays a pivotal role in tumor propagation by preventing premature interaction between MK and LRP1, we performed knockdown experiments for RAP of the human colorectal adenocarcinoma cell line SW620. Successful knockdown of RAP resulted in intracellular retention of MK and suppression of MK secretion and consequently in the suppression of cell survival under low serum conditions (Fig. 5*D*).

DISCUSSION

Since the initial proposal of the concept of "autocrine secretion" by Sporn and Todaro (31), an increasing body of evidence has confirmed its biological significance. In the late 1980s, a biologically productive premature interaction, *i.e.* signal transduction via intracellular ligand-receptor binding, was reported for artificially ER-retained interleukin-3 and PDGF (32–34). These were the first demonstration that the premature interaction might have a biological role. However, our present data appear to be in conflict with these reports. The importance of our findings is that a growth factor and its receptor come to contact during biosynthesis, and this premature interaction negatively regulates their production within the secretory pathway. Avoiding this premature interaction may allow cells to overproduce a growth factor and thus to acquire a growth advantage. Indeed, here, we found that the LRP chaperone RAP blocks the premature MK-LRP1 interaction/aggregate formation and that increased RAP expression is closely associated with MK expression in human colorectal carcinomas. Consistent with this, serum MK levels have been shown to be elevated in human colorectal carcinoma patients (10). Thus, our findings highlight the biological significance of a premature interaction in the autocrine secretory pathway.

LRP1 is the fastest endocytosis receptor among the LDL receptor family members (35), and its endocytosis-dependent function has been intensively studied. For example, it has been

Downloaded from www.jbc.org at NAGOYA UNIV CENTRAL LIBRARY, on March 6, 2012

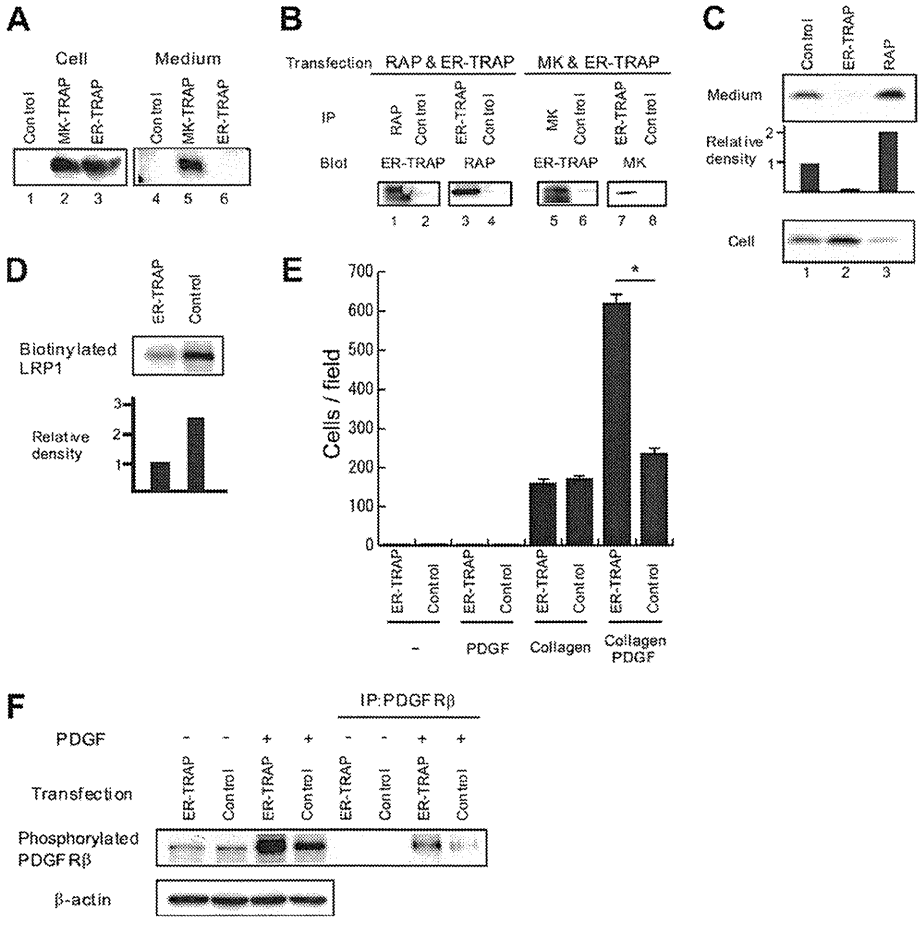

FIGURE 4. **ER-TRAP traps MK in the cell.** *A*, the indicated expression vectors were transfected into CHO K1 cells. Proteins from cell lysates or media were subjected to Western blot analysis with anti-HA antibody that recognizes MK-TRAP and ER-TRAP. *B*, the indicated expression vectors were transfected into CHO K1 cells. Anti-HA and anti-FLAG antibodies were used to detect ER-TRAP and RAP, respectively. *C*, an MK-vector was co-transfected with the indicated expression vectors into CHO-mLRP-IV cells. Proteins were then detected by Western blot analysis. *D*, NIH3T3 cells were transfected with ER-TRAP or control vector. Cell surface proteins were labeled with biotin, immunoprecipitated (*IP*) with anti-LRP1 antibody, and separated under 5% SDS-PAGE. Biotinylated LRP1 was detected with HRP-conjugated streptavidin. *E*, NIH3T3 cells were transfected with ER-TRAP or control vector. Cell migration analysis was then performed. *, $p < 0.001$ (Student's *t* test). *F*, NIH3T3 cells transfected with ER-TRAP or control vector were incubated in 0.2% BSA in DMEM for 3 h and stimulated with 50 ng/ml PDGF-BB for 10 min. Phosphorylation of PDGF receptor was detected with anti-phosphotyrosine antibody (Tyr(P)-100).

determined that LRP1-mediated endocytosis of MK leads to nuclear targeting by endocytosed MK, which is, at least in part, responsible for MK-induced cell survival (22). The production and clearance of amyloid-β (Aβ), a pathogenic peptide of Alzheimer disease, are also dependent on the LRP1-mediated endocytosis. Thus, amyloid precursor protein (APP), a membrane protein, is intracellularly bridged with LRP1 by FE65 (36, 37). APP also binds to LRP1 extracellularly (38). The consequent APP-LRP1 complex is endocytosed and is further processed to produce Aβ. In regard to clearance of Aβ, extracellular Aβ binds directly to LRP1 and also binds indirectly to LRP1 through Aβ-binding molecules, including apoE (39–41); after these interactions, the Aβ is degraded intracellularly. In this context, our study has highlighted another function of LRP1, *i.e.* regulation of ligand biosynthesis. To the best of our knowledge, this is the first demonstration of a receptor playing an essential role in the biosynthesis of its ligand. We demonstrated that MK overexpression leads to the formation of aggregates between MK and LRP1, thereby suppressing MK secretion. Endogenous MK induced by retinoic acid treatment is also co-localized with LRP1 within the cell and thus is not secreted. The premature MK-LRP interaction may occur under both physiological and pathological conditions. It is conceivable that MK secretion may parallel its mRNA and protein expression until RAP is capable of blocking the premature MK-LRP1 interaction, but it may be impaired once MK protein expression overcomes RAP capacity (Fig. 6).

MK and apoE are LRP1 ligands. Interestingly, both MK and apoE can bind to Aβ, and MK, apoE, and LRP1 are found in senile plaques (39, 41–44). In addition, MK and apoE also show similar characteristics from the point of view of premature interaction with LRP1: overexpression of apoE or MK suppresses LRP1 maturation and induces LRP1 aggregation, which is restored by RAP expression (20; this study). In contrast, we found that the associated protein expressions are observed for RAP and MK, but not apoE, in human colorectal carcinomas. This indicates that MK and apoE have distinct biological significance and suggests that the biosyntheses of MK and apoE are differentially regulated, at least in these cancer cells.

Downloaded from www.jbc.org at NAGOYA UNIV CENTRAL LIBRARY, on March 6, 2012

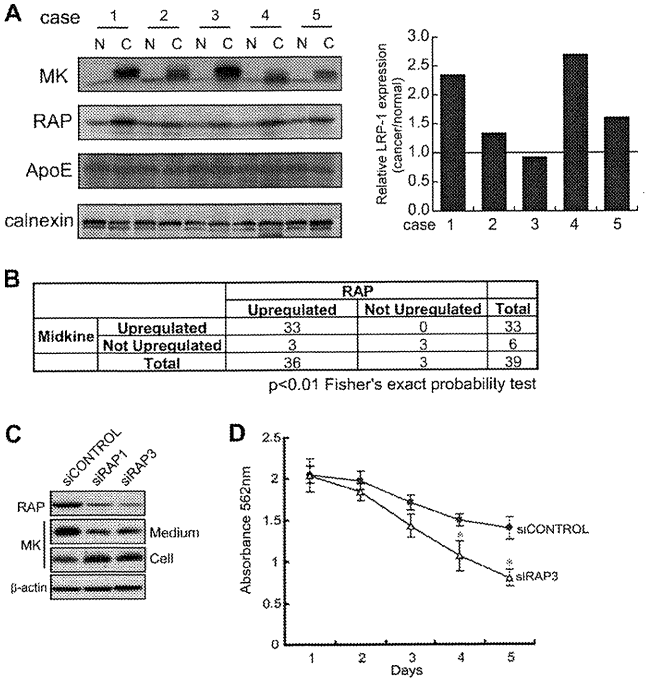

FIGURE 5. **Productions of MK and RAP are closely associated in human colorectal carcinomas.** *A*, human colorectal carcinomas and adjacent normal tissues were subjected to Western blot analysis for MK, RAP, apoE, and calnexin protein expression and quantitative real-time RT-PCR for LRP1 mRNA expression. Five of 39 cases examined are shown here. *C*, carcinoma tissue; *N*, adjacent normal tissue. *B*, statistical analysis. *C*, SW620 cells were transfected with the indicated siRNAs. After 48 h, cells were harvested, and proteins were analyzed by immunoblotting. *D*, SW620 cells transfected with the indicated siRNAs were seeded, and the cell numbers were monitored by 3-(4,5-dimethylthiazol-2-yl)-2,5-diphenyltetrazolium bromide (MTT) assay. *, $p < 0.01$ (*t* test). siRAP1 also gave similar results with siRAP3 (data not shown).

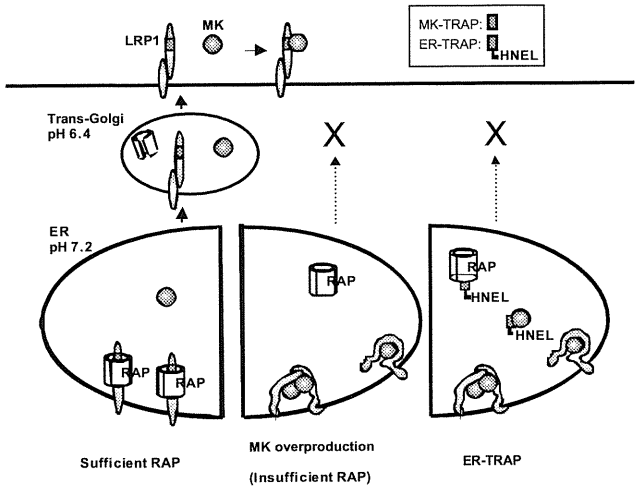

FIGURE 6. **Mechanisms of biosynthetic regulation for MK and LRP1.** Under physiological conditions, RAP promotes folding of LRP1 and prevents premature interaction between LRP1 and MK. If RAP becomes insufficient under pathological conditions, such as overproduction of MK during carcinogenesis, aggregate formation involving LRP1 and MK takes place. ER-TRAP may competitively occupy RAP, leading to aggregate formation of LRP1. ER-TRAP also directly binds and traps MK in the ER. Consequently, ER-TRAP suppresses both LRP1 maturation and MK secretion. MK-TRAP is the N-terminal half of the second ligand-binding domain of LRP1, which corresponds to SLRP2N-EGF (see "Experimental Procedures"). ER-TRAP is the MK-TRAP plus HNEL (an ER-retrieving signal).

It should be noted that other LRP1 ligands, such as tPA, urokinase, and plasminogen activator inhibitor-1, do not induce LRP1 aggregation (20). As discussed previously (20), formation of ligand-receptor aggregation may require polymerization of the ligand itself and/or ability of the ligand to bind to multiple ligand-binding domains of the receptor. A previous study reported that MK forms a homodimer (45), and our present data indicate that MK binds to the second and fourth ligand-binding domains of LRP1. It is known that apoE can form small multivalent lipoprotein particles and binds to three ligand-binding domains of LRP1. In contrast, tPA and PAI-1 may bind to a single site of LRP1 (46). This could be a reason why MK forms an aggregate with LRP1 within the secretory pathway. However, the precise mechanisms underlying the premature ligand-LRP1 interaction remain to be elucidated.

The results of ER-TRAP not only support the significance of the premature interaction in the biosynthesis of MK and LRP1, but also provide an intriguing strategy by which simultaneous repression of a growth factor and its receptor can be achieved. This strategy allows efficient trapping of a growth factor and a chaperone specialized for its receptor within the ER (Fig. 6). It may be applicable to certain disease treatments aimed at the suppression of ligand and/or receptor expression.

Acknowledgments—We thank Sachie Shimada, Miho Okada, Motoki Sato, and Junna Yamaguchi for excellent technical assistance in the initial stage of this study.

REFERENCES

1. Sporn, M. B., and Roberts, A. B. (1992) *Ann. Intern. Med.* **117,** 408–414
2. Kadomatsu, K., Tomomura, M., and Muramatsu, T. (1988) *Biochem. Biophys. Res. Commun.* **151,** 1312–1318
3. Tomomura, M., Kadomatsu, K., Matsubara, S., and Muramatsu, T. (1990) *J. Biol. Chem.* **265,** 10765–10770
4. Rauvala, H., Huttunen, H. J., Fages, C., Kaksonen, M., Kinnunen, T., Imai, S., Raulo, E., and Kilpeläinen, I. (2000) *Matrix Biol.* **19,** 377–387
5. Deuel, T. F., Zhang, N., Yeh, H. J., Silos-Santiago, I., and Wang, Z. Y. (2002) *Arch. Biochem. Biophys.* **397,** 162–171
6. Kadomatsu, K., and Muramatsu, T. (2004) *Cancer Lett.* **204,** 127–143
7. Horiba, M., Kadomatsu, K., Nakamura, E., Muramatsu, H., Ikematsu, S., Sakuma, S., Hayashi, K., Yuzawa, Y., Matsuo, S., Kuzuya, M., Kaname, T., Hirai, M., Saito, H., and Muramatsu, T. (2000) *J. Clin. Invest.* **105,** 489–495
8. Hobo, A., Yuzawa, Y., Kosugi, T., Kato, N., Asai, N., Sato, W., Maruyama, S., Ito, Y., Kobori, H., Ikematsu, S., Nishiyama, A., Matsuo, S., and Kadomatsu, K. (2009) *J. Clin. Invest.* **119,** 1616–1625
9. Tsutsui, J., Kadomatsu, K., Matsubara, S., Nakagawara, A., Hamanoue, M., Takao, S., Shimazu, H., Ohi, Y., and Muramatsu, T. (1993) *Cancer Res.* **53,** 1281–1285
10. Ikematsu, S., Yano, A., Aridome, K., Kikuchi, M., Kumai, H., Nagano, H., Okamoto, K., Oda, M., Sakuma, S., Aikou, T., Muramatsu, H., Kadomatsu, K., and Muramatsu, T. (2000) *Br. J. Cancer* **83,** 701–706
11. Nakagawara, A., Milbrandt, J., Muramatsu, T., Deuel, T. F., Zhao, H., Cnaan, A., and Brodeur, G. M. (1995) *Cancer Res.* **55,** 1792–1797
12. Mashour, G. A., Ratner, N., Khan, G. A., Wang, H. L., Martuza, R. L., and Kurtz, A. (2001) *Oncogene* **20,** 97–105
13. Ikematsu, S., Nakagawara, A., Nakamura, Y., Sakuma, S., Wakai, K., Muramatsu, T., and Kadomatsu, K. (2003) *Br. J. Cancer* **88,** 1522–1526
14. Takei, Y., Kadomatsu, K., Matsuo, S., Itoh, H., Nakazawa, K., Kubota, S., and Muramatsu, T. (2001) *Cancer Res.* **61,** 8486–8491
15. Takei, Y., Kadomatsu, K., Goto, T., and Muramatsu, T. (2006) *Cancer* **107,** 864–873

Downloaded from www.jbc.org at NAGOYA UNIV CENTRAL LIBRARY, on March 6, 2012

16. Herz, J., and Strickland, D. K. (2001) *J. Clin. Invest.* **108,** 779–784
17. Herz, J., Clouthier, D. E., and Hammer, R. E. (1992) *Cell* **71,** 411–421
18. Bu, G., Geuze, H. J., Strous, G. J., and Schwartz, A. L. (1995) *EMBO J.* **14,** 2269–2280
19. Bu, G., and Rennke, S. (1996) *J. Biol. Chem.* **271,** 22218–22224
20. Willnow, T. E., Rohlmann, A., Horton, J., Otani, H., Braun, J. R., Hammer, R. E., and Herz, J. (1996) *EMBO J.* **15,** 2632–2639
21. Muramatsu, H., Zou, K., Sakaguchi, N., Ikematsu, S., Sakuma, S., and Muramatsu, T. (2000) *Biochem. Biophys. Res. Commun.* **270,** 936–941
22. Shibata, Y., Muramatsu, T., Hirai, M., Inui, T., Kimura, T., Saito, H., McCormick, L. M., Bu, G., and Kadomatsu, K. (2002) *Mol. Cell. Biol.* **22,** 6788–6796
23. Li, Y., Marzolo, M. P., van Kerkhof, P., Strous, G. J., and Bu, G. (2000) *J. Biol. Chem.* **275,** 17187–17194
24. Obermoeller-McCormick, L. M., Li, Y., Osaka, H., FitzGerald, D. J., Schwartz, A. L., and Bu, G. (2001) *J. Cell Sci.* **114,** 899–908
25. Obermoeller, L. M., Warshawsky, I., Wardell, M. R., and Bu, G. (1997) *J. Biol. Chem.* **272,** 10761–10768
26. Ye, C., Qi, M., Fan, Q. W., Ito, K., Akiyama, S., Kasai, Y., Matsuyama, M., Muramatsu, T., and Kadomatsu, K. (1999) *Br. J. Cancer* **79,** 179–184
27. Chen, S., Bu, G., Takei, Y., Sakamoto, K., Ikematsu, S., Muramatsu, T., and Kadomatsu, K. (2007) *J. Cell Sci.* **120,** 4009–4015
28. Frisch, S. M., and Screaton, R. A. (2001) *Curr. Opin. Cell Biol.* **13,** 555–562
29. Obermoeller, L. M., Chen, Z., Schwartz, A. L., and Bu, G. (1998) *J. Biol. Chem.* **273,** 22374–22381
30. Boucher, P., Gotthardt, M., Li, W. P., Anderson, R. G., and Herz, J. (2003) *Science* **300,** 329–332
31. Sporn, M. B., and Todaro, G. J. (1980) *N. Engl. J. Med.* **303,** 878–880
32. Keating, M. T., and Williams, L. T. (1988) *Science* **239,** 914–916
33. Dunbar, C. E., Browder, T. M., Abrams, J. S., and Nienhuis, A. W. (1989) *Science* **245,** 1493–1496
34. Bejcek, B. E., Li, D. Y., and Deuel, T. F. (1989) *Science* **245,** 1496–1499
35. Li, Y., Lu, W., Marzolo, M. P., and Bu, G. (2001) *J. Biol. Chem.* **276,** 18000–18006
36. Trommsdorff, M., Borg, J. P., Margolis, B., and Herz, J. (1998) *J. Biol. Chem.* **273,** 33556–33560
37. Pietrzik, C. U., Yoon, I. S., Jaeger, S., Busse, T., Weggen, S., and Koo, E. H. (2004) *J. Neurosci.* **24,** 4259–4265
38. Kounnas, M. Z., Moir, R. D., Rebeck, G. W., Bush, A. I., Argraves, W. S., Tanzi, R. E., Hyman, B. T., and Strickland, D. K. (1995) *Cell* **82,** 331–340
39. Strittmatter, W. J., Weisgraber, K. H., Huang, D. Y., Dong, L. M., Salvesen, G. S., Pericak-Vance, M., Schmechel, D., Saunders, A. M., Goldgaber, D., and Roses, A. D. (1993) *Proc. Natl. Acad. Sci. U.S.A.* **90,** 8098–8102
40. Deane, R., Wu, Z., Sagare, A., Davis, J., Du Yan, S., Hamm, K., Xu, F., Parisi, M., LaRue, B., Hu, H. W., Spijkers, P., Guo, H., Song, X., Lenting, P. J., Van Nostrand, W. E., and Zlokovic, B. V. (2004) *Neuron* **43,** 333–344
41. Tamamizu-Kato, S., Cohen, J. K., Drake, C. B., Kosaraju, M. G., Drury, J., and Narayanaswami, V. (2008) *Biochemistry* **47,** 5225–5234
42. Yasuhara, O., Muramatsu, H., Kim, S. U., Muramatsu, T., Maruta, H., and McGeer, P. L. (1993) *Biochem. Biophys. Res. Commun.* **192,** 246–251
43. Strittmatter, W. J., Saunders, A. M., Schmechel, D., Pericak-Vance, M., Enghild, J., Salvesen, G. S., and Roses, A. D. (1993) *Proc. Natl. Acad. Sci. U.S.A.* **90,** 1977–1981
44. Rebeck, G. W., Reiter, J. S., Strickland, D. K., and Hyman, B. T. (1993) *Neuron* **11,** 575–580
45. Kojima, S., Muramatsu, H., Amanuma, H., and Muramatsu, T. (1995) *J. Biol. Chem.* **270,** 9590–9596
46. Willnow, T. E., Orth, K., and Herz, J. (1994) *J. Biol. Chem.* **269,** 15827–15832

Downloaded from www.jbc.org at NAGOYA UNIV CENTRAL LIBRARY, on March 6, 2012

The American Journal of Pathology, Vol. 178, No. 2, February 2011
Copyright © 2011 American Society for Investigative Pathology.
Published by Elsevier Inc. All rights reserved.
DOI: 10.1016/j.ajpath.2010.10.009

Cardiovascular, Pulmonary, and Renal Pathology

Basigin/CD147 Promotes Renal Fibrosis after Unilateral Ureteral Obstruction

Noritoshi Kato,*† Tomoki Kosugi,*† Waichi Sato,† Takuji Ishimoto,† Hiroshi Kojima,† Yuka Sato,† Kazuma Sakamoto,* Shoichi Maruyama,† Yukio Yuzawa,† Seiichi Matsuo,† and Kenji Kadomatsu*

From the Departments of Biochemistry and Nephrology of Internal Medicine,† Nagoya University Graduate School of Medicine, Nagoya, Japan*

Regardless of their primary causes, progressive renal fibrosis and tubular atrophy are the main predictors of progression to end-stage renal disease. Basigin/CD147 is a multifunctional molecule–it induces matrix metalloproteinases and hyaluronan, for example–and has been implicated in organ fibrosis. However, the relationship between basigin and organ fibrosis has been poorly studied. We investigated basigin's role in renal fibrosis using a unilateral ureteral obstruction model. Basigin-deficient mice ($Bsg^{-/-}$) demonstrated significantly less fibrosis after surgery than $Bsg^{+/+}$ mice. Fewer macrophages had infiltrated in $Bsg^{-/-}$ kidneys. Consistent with these *in vivo* data, primary cultured tubular epithelial cells from $Bsg^{-/-}$ mice produced less matrix metalloproteinase and exhibited less motility on stimulation with transforming growth factor β. Furthermore, $Bsg^{-/-}$ embryonic fibro blasts produced less hyaluronan and α-smooth muscle actin after transforming growth factor β stimulation. Together, these results demonstrate for the first time that basigin is a key regulator of renal fibrosis. Basigin could be a candidate target molecule for the prevention of organ fibrosis. *(Am J Pathol 2011, 178:572–579; DOI: 10.1016/j.ajpath.2010.10.009)*

Regardless of the primary disease process, renal interstitial fibrosis is the key determinant of chronically diseased kidney and the main prognostic predictor of renal function.[1] Excessive accumulation of extracellular matrix (ECM) leads to dysfunction of the organ and state of fibrosis.[2] ECM turnover is regulated by the activity of matrix metalloproteinases (MMPs). Although transforming growth factor β (TGF-β) stimulates α-SMA expression as well as ECM production by fibroblasts, it also regulates the expression of MMPs.[3,4] Conversely, some MMPs, such as MMP-2, MMP-9, and MT1-MMP, activate latent TGF-β.[5,6] Therefore, ECM synthesis and degradation are intricately regulated by TGF-β, MMPs, and others. In this context, it should also be noted that hyaluronan plays a crucial role in the TGF-β–driven differentiation of fibroblasts into myofibroblasts.[7–10] Endogenous hyaluronan is necessary for fibroblast differentiation and maintenance of the myofibroblast phenotype through autocrine TGF-β action.[11]

Basigin (Bsg)/CD147 (*Bsg* is the name of the mouse gene) is a glycosylated transmembrane protein that belongs to the immunoglobulin superfamily. It is expressed by many types of cells, including hematopoietic, epithelial, endothelial, and tumor cells.[12,13] It is well documented that Bsg induces MMPs, so it is also known as an extracellular matrix metalloproteinase inducer (EMMPRIN).[14] It is highly up-regulated in many malignant cancer cells and is thought to contribute to cell survival, invasion, metastasis, and multidrug resistance.[15] Studies targeting Bsg to prevent tumor growth using RNAi techniques have achieved successful outcomes.[16–19] Along with MMPs, Bsg is also involved in the production of vascular endothelial growth factor and hyaluronan.[20–24] Bsg interacts with a wide range of binding partners.[25] For example, it binds to caveolin, cyclophilin, monocarboxylate transporter, and Bsg itself.[26–29] Through the interaction with monocarboxylate transporter, Bsg plays a role in lactate metabolism. Furthermore, Bsg promotes the differentiation of fibroblasts into myofibroblasts by inducing α-SMA expression in corneal fibroblasts.[30]

We previously generated Bsg-deficient mice ($Bsg^{-/-}$) and reported several abnormalities, including male and female sterility, progressive retinal degeneration, increased cell proliferation on mixed lymphocyte culture, decreased

Supported by Grants-in-Aid from the Ministry of Education, Culture, Sports, Science, and Technology of Japan (the global COE program to Nagoya University).

Accepted for publication October 1, 2010.

N.K. and T.K. contributed equally to this work.

Address reprint requests to Kenji Kadomatsu, M.D., Ph.D., Department of Biochemistry, Nagoya University Graduate School of Medicine, 65 Tsurumai-cho, Showa-ku, Nagoya 466-8550, Japan. E-mail: kkadoma@med.nagoya-u.ac.jp.

memory function, and abnormal sensory function.[31–33] Most recently, we also found that Bsg is an E-selectin ligand and is involved in renal ischemia/reperfusion injury.[34]

In this study, we focused on Bsg functions in renal fibrosis induced by unilateral ureteral obstruction (UUO). Bsg orchestrates renal fibrosis formation through MMPs, hyaluronan production, and macrophage infiltration. To the best of our knowledge, this is the first report on the critical role of Bsg in renal fibrosis.

Materials and Methods

Animals and Experimental Design

Mice deficient in *Bsg* were generated as described previously.[35] Because $Bsg^{-/-}$ mice were hardly born through ordinary mating, we established the following protocol. $Bsg^{+/-}$ mice with 129/SV background were backcrossed with C57BL/6J mice to produce F1 hybrid offspring (reverse F1 hybrid). By intercrossing these mice, mixed reverse F2 mice were generated, and were used in this study. All experiments were performed with $Bsg^{+/+}$ and $Bsg^{-/-}$ littermates. We used 96 mice (48 mice in each genotype, respectively), which were 8- to 12-week-old males weighing 20 to 25 g. These mice were divided into seven groups at each time point (n = 8/each group on day 0, 7, and 14; n = 6/each group on day 1, 2, 3, and 5, respectively). The mice were housed under controlled environmental conditions and maintained with standard food and water.

In $Bsg^{+/+}$ and $Bsg^{-/-}$ mice sedated by general anesthesia, an incision was made in the right side of the back, and complete ureteral obstruction was performed by double-ligating the right ureter using 4-0 silk. Sham-operated mice had their ureters exposed but not ligated. Mice were sacrificed at different time points as indicated after surgery. Kidneys were removed for examination. Blood and urine samples were collected on the day of sacrifice. Kidney tissues were processed for histology and protein extraction. All of the animal experiments were performed in accordance with the animal experimentation guidelines of Nagoya University School of Medicine.

Histology

The removed kidneys were fixed in 4% paraformaldehyde, embedded in paraffin, and then cut into 4-μm sections. The sections were stained with polyclonal goat anti-human type III collagen (Southern Biotech, Birmingham, AL) and polyclonal goat anti-mouse Bsg (R&D Systems, Minneapolis, MN) followed by detection with biotin-conjugated rabbit anti-goat IgG (Nichirei, Tokyo, Japan). Immunostaining was performed by the streptavidin (Chemicon International, Temecula, CA) -biotin immunoperoxidase method. The staining was visualized with 3,3′-diaminobenzidine (Dako, Carpinteria, CA), a brown color being produced. Negative controls involved replacement of the primary antibodies with species-matched antibodies.

The sections were stained with periodic acid-Schiff reagent (PAS). Tubular dilation was assessed by counting the number of dilated tubules in the cortex of each section.[36] They were also stained with a terminal deoxynucleotidyl transferase-mediated dUTP nick-end labeling (TUNEL) assay kit according to the manufacturer's instructions (Roche Applied Science, Indianapolis, IN). The number of apoptotic cells was examined in the cortex of each section.

Parts of the kidney tissues were snap-frozen in liquid nitrogen. Sections (2-μm thick) were cut with a cryostat and then fixed in acetone. The cryosections were stained with rat anti-mouse monocyte-macrophage marker F4/80 (Serotec, Oxford, UK) followed by detection with fluorescein isothiocyanate rabbit anti-rat IgG (Zymed Laboratories, San Francisco, CA). Macrophages positive for F4/80 were counted by examining 10 fields of the cortex under a microscope at ×200 magnification in a blind manner.

Real-Time PCR

Mouse kidney tissues were snap-frozen in liquid nitrogen for total mRNA isolation. To perform mRNA extraction and cDNA synthesis, we used the RNeasy Mini Kit and QuantiTect Reverse Transcriptional Kit (Qiagen, Hilden, Germany) according to the manufacturer's instructions. Real-time PCR analysis was performed with an Applied Biosystems Prism 7500HT sequence detection system using TaqMan gene expression assays according to the manufacturer's specifications (Applied Biosystems, Foster City, CA). TaqMan probes and primers for type III collagen (Col3a1; Mm00802331_m1), TGF-β_1 (*Tgfb1*; Mm00441724_m1), hyaluronan synthase 2 (*Has2*; Mm00515089_m1), α-SMA (*Acta2*; Mm01546133_m1), β-actin (*Actb*; Mm00607939_s1), and glyceraldehyde-3-phosphate dehydrogenase (*Gapdh*; Mm99999915_g1) were used. Amplification data were analyzed with Applied Biosystems Sequence Detection software version 1.3.1.

Western Blot Analysis

Mouse kidney tissues were snap-frozen in liquid nitrogen for protein isolation and then lysed in radio-immunoprecipitation assay buffer (50 mmol/L Tris-HCl, 150 mmol/L NaCl, 1% Nonidet P, 1% deoxycolic acid, and 0.05% SDS). Western blot analysis was performed as described previously.[37]

Briefly, we separated the samples by 10% SDS-PAGE and then transferred them to a nitrocellulose membrane (Whatman, Florham Park, NJ). We blocked the membranes with 5% (w/v) dry fat-free milk in PBS with 0.1% Tween for 60 minutes at room temperature. The blots were subsequently incubated with goat anti-mouse Bsg antibody (R&D Systems), monoclonal anti-β actin antibody (Sigma Aldrich, St. Louis, MO), or rat anti-mouse E-selectin antibody (R&D Systems), followed by incubation with peroxidase-conjugated anti-goat IgG, rat IgG, and mouse IgG (Jackson Immunoresearch Laboratories, West Grove, PA). Proteins were visualized with an enhanced chemiluminescence detection system (Amersham Pharmacia, Amersham Biosciences, Piscataway, NJ). The density of each band was measured using the public domain National Institutes of Health image program.

Gelatin Zymography

Kidney tissue homogenates and cultured media of TECs were subjected to gelatin zymography of the MMP proteolytic activity. Gelatin zymography was performed using commercial kit (Invitrogen, Carlsbad, CA) according to the manufacturer's instructions. Briefly, the homogenates were loaded into 7.5% SDS-polyacrylamide gel containing 1 mg/ml gelatin. After electrophoresis, the gel was incubated in 2.5% Triton X-100 at room temperature for 30 minutes with gentle shaking and then at 37°C for 24 hours in a developing buffer containing $CaCl_2$ Tris-HCl. The gel was stained with Coomassie blue. Proteinase activity was detected as unstained bands on a blue background, representing areas of gelatin digestion. The density of each band was measured using the public-domain National Institutes of Health image program.

Cell Culture

Tubular epithelial cells (TECs) were isolated from the kidneys of adult $Bsg^{+/+}$ or $Bsg^{-/-}$ mice, as described previously.[38] Briefly, the renal cortex divided from the medulla was resolved with collagenase (Wako Chemicals, Miyazaki, Japan) and the lysate was then filtered through 38-μm strainer, using a mesh sieving method. The fluid was centrifuged to pellet the various renal cells, which were plated with cultured media for 1 hour of incubation. To avoid the contamination of mesangial cells and various cells, adherent cells were removed, and a supernatant solution including numerous TECs was incubated to another plate for 72 hours in K1 medium [224.25 ml Ham's F12; 226.25 ml Dulbecco's modified Eagle's medium (DMEM); and 12.5 ml HEPES] containing 10% fetal bovine serum (GIBCO BRL, Gaithersburg, MD) and hormones [epidermal growth factor (50 pg/ml); insulin-transferrin-sodium selenite media supplement (0.12 IU/ml), prostaglandin E_1 (1.25 ng/ml), hydrocortisone (18 ng/ml); T3 (34 pg/ml)]. The fourth and fifth passages were used for experiments. These cells isolated from the kidneys were determined to be of proximal tubular origin by means of immunofluorescence histochemistry; cells were stained positively for cytokeratin (ENZO Diagnostics, Farmingdale, NY); brush border vesicle (BBV; gift from Dr. G. Andres)[39]; desmin (Progen, Heidelberg, Germany), and Phalloidin (Invitrogen). These staining patterns were the same as those previously reported.[40]

Subconfluent tubular epithelial cells were incubated in serum-free medium for 24 hours to arrest and synchronize cell growth. After that, the medium was changed to fresh serum-free DMEM containing 5 ng/ml recombinant TGF-β (R&D Systems) for 0, 1, 3, 6, 12, and 24 hours in the time-course study. *The culture* medium was subjected to gelatin zymography.

Mouse embryonic fibroblast (MEF) was established from the embryos of $Bsg^{+/+}$ and $Bsg^{-/-}$ mice and then cultured in DMEM containing 10% fetal bovine serum.[41] After the cells were starved for 24 hours, the medium was changed to fresh serum-free DMEM containing 5 ng/ml recombinant TGF-β (R&D Systems). Cells were then used for the collection of mRNA, and culture medium was used for hyaluronan ELISA.

Cell Invasion Assay

To compare cell migration capacity between $Bsg^{+/+}$ TECs and $Bsg^{-/-}$, we used the Cultrex Cell Invasion/Migration Assay according to the manufacturer's instructions (Trevigen, Gaithersburg, MD) to mimic *in vivo* the tubular basement membrane microenvironment and the renal interstitium and to screen compounds that influence cellular digestion and migration across ECM. This assay used a simplified Boyden chamber design with an 8-micron polyethylene terephthalate membrane coated with basement membrane extract. The bottom wells of a 96-well Boyden chamber were filled with DMEM containing 5 ng/ml TGF-β (R&D Systems). $Bsg^{+/+}$ and $Bsg^{-/-}$ TECs were labeled with calcein-AM beforehand, and then 5.0×10^4 cells/well were added to the upper chamber. The Boyden chamber was incubated for 24 hours at 37°C to allow the possible migration of cells into the lower chamber. The number of migrated cells was estimated as fluorescence using Fluoroskan AscentCF (Labsystems, Helsinki, Finland).

Statistical Analysis

All values are expressed as means ± SD. Statistical analysis was performed with the unpaired, two-tailed Student's *t*-test for single comparisons. Values of $P < 0.05$ were considered to indicate statistically significant differences.

Results

$Bsg^{-/-}$ *Mice Have Less Tubulointerstitial Fibrosis*

To determine the role of Bsg in renal fibrosis, we subjected $Bsg^{+/+}$ and $Bsg^{-/-}$ mice to UUO surgery and compared the degrees of type III collagen deposition in the tubulointerstitium. At 7 days after UUO operation, both genotypes exhibited increased expression of type III collagen on immunohistochemistry (Figure 1A). This deposition became more diffuse and remarkable at 14 days in the interstitium of $Bsg^{+/+}$ mice, whereas $Bsg^{-/-}$ mice showed only a little more fibrosis. Consistent with the immunohistochemical findings, type III collagen mRNA expression also increased at 14 days in $Bsg^{+/+}$ mice compared with $Bsg^{-/-}$ mice, which was revealed by quantitative RT-PCR (Figure 1B).

PAS staining revealed marked tubular dilation and atrophy in both genotypes at 14 days (Figure 1C). It is likely that the infiltration of inflammatory cells was prominent in $Bsg^{+/+}$ mice. To verify the tubular damage, we assessed the number of dilated tubules at 7 and 14 days. There was no significant difference between the two genotypes (Figure 1D), suggesting that both groups operated on had the same extent of renal

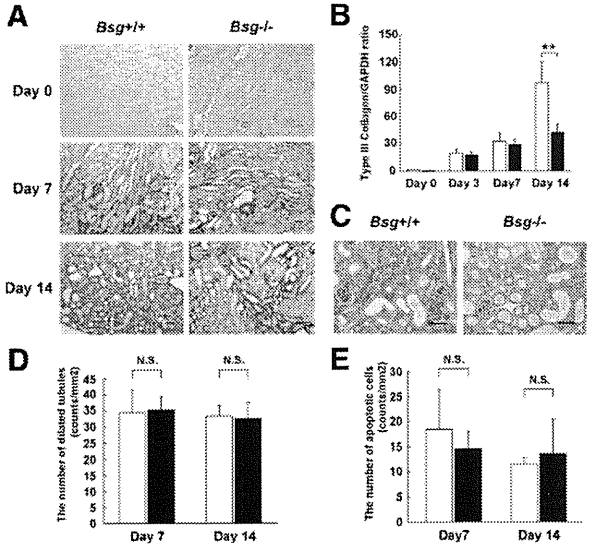

Figure 1. Histological evaluation of the kidneys of $Bsg^{+/+}$ and $Bsg^{-/-}$ mice after UUO. **A:** Type III collagen expression in the tubulointerstitium at 0, 7, and 14 days after UUO operation. Scale bar = 50 μm. **B:** Type III collagen mRNA expression, determined by quantitative reverse transcriptase PCR. Each value was standardized by GAPDH mRNA content as an internal control. Data are means (columns) ± SD (bars); white bar, $Bsg^{+/+}$; black bar, $Bsg^{-/-}$; $^{**}P < 0.01$; $n = 6$. **C:** The tubulointerstitium at 14 days is shown by PAS staining. Scale bar = 50 μm. **D:** The number of dilated tubules (counts/mm^2). Data are means ± SD; white bar, $Bsg^{+/+}$; black bar, $Bsg^{-/-}$; N.S., not significant; $n = 8$. **E:** The number of apoptotic cells (counts/mm^2), assessed by TUNEL assay. Data are means ± SD; white bar, $Bsg+/+$; black bar, $Bsg^{-/-}$; $n = 8$.

damage. We further performed TUNEL assay to examine the effect of Bsg on apoptosis of tubular injuries. But, no obvious difference was observed between the two genotypes (Figure 1E).

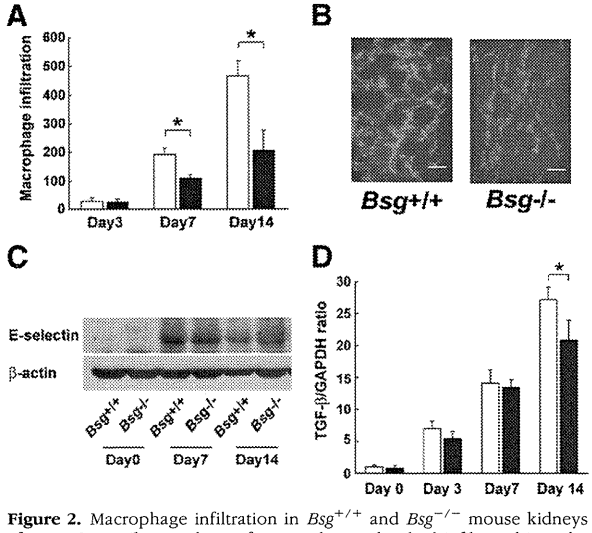

Figure 2. Macrophage infiltration in $Bsg^{+/+}$ and $Bsg^{-/-}$ mouse kidneys after UUO. **A:** The numbers of macrophages that had infiltrated into the tubulointerstitium at 3, 7, and 14 days were counted. Data are means ± SD; white bar, $Bsg^{+/+}$; black bar, $Bsg^{-/-}$; $^{*}P < 0.05$; $n = 6$. **B:** Immunofluorescence staining with F4/80 antibody at 7 days. Scale bar = 50 μm. **C:** Western blotting of E-selectin expression in the kidney after UUO. **D:** TGF-β mRNA, determined by real-time PCR. Each value was standardized by GAPDH mRNA content as an internal control. Data are means ± SD; white bar, $Bsg^{+/+}$; black bar, $Bsg^{-/-}$; $^{*}P < 0.05$; $n = 6$.

Macrophage Infiltration Is Lower in Bsg$^{-/-}$ *Mice*

Macrophage infiltration is a key event for the pathogenesis of renal fibrosis.[42,43] Both $Bsg^{+/+}$ and $Bsg^{-/-}$ mice exhibited only slight macrophage infiltration at day 3 (Figure 2A). Macrophage infiltration into the interstitium became prominent at day 7, and increased more at day 14 (Figure 2, A and B). The infiltrating macrophage number was significantly higher in the $Bsg^{+/+}$ kidneys (Figure 2A).

Macrophage infiltration in the post-obstructed kidney requires adhesion molecules.[44] However, little information about E-selectin is available. Because Bsg acts as an E-selectin ligand on inflammatory cells,[34] we next examined E-selectin expression in the kidney. We found that E-selectin expression was upregulated in the kidney after UUO surgery, but the expression levels were comparable between the genotypes (Figure 2C).

TGF-β serves as a profibrogenic cytokine by directly stimulating the synthesis of extracellular matrix components and indirectly stimulating other profibrogenic factors such as connective tissue growth factor.[45] TGF-β is produced by many types of cells in the UUO model, and

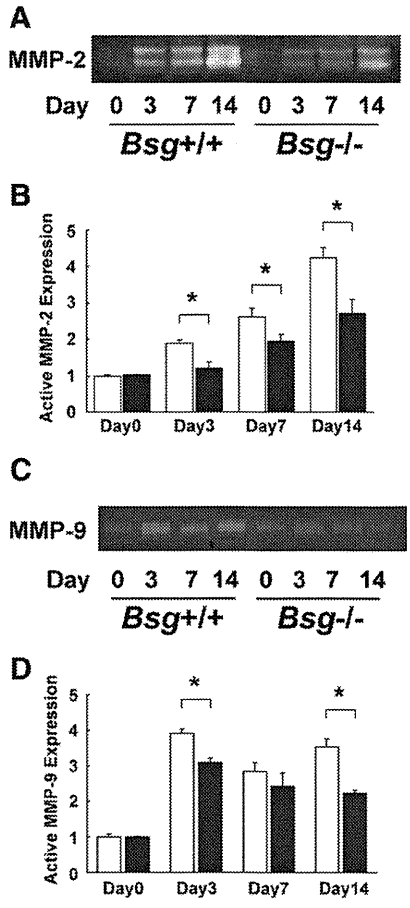

Figure 3. Induction of renal MMPs in the $Bsg^{+/+}$ and $Bsg^{-/-}$ mouse kidneys after UUO. **A:** Zymographic analysis of whole kidney lysates indicating MMP-2 induction. **B:** The intensity of active-MMP-2 bands. Data are means ± SD; white bar, $Bsg^{+/+}$; black bar, $Bsg^{-/-}$; $^{*}P < 0.05$; $n = 6$. **C:** A representative photo of MMP-9 activation in gelatin zymography. **D:** The intensity of active-MMP-9 bands. Data are means ± SD; white bar, $Bsg^{+/+}$; black bar, $Bsg^{-/-}$; $^{*}P < 0.05$; $n = 6$.

macrophage is one of the major sources.[42,45] We found that TGF-β was equally up-regulated in both genotypes until 7 days after UUO surgery (Figure 2D). Then TGF-β expression in $Bsg^{+/+}$ exceeded that in $Bsg^{-/-}$ mice at day 14 (Figure 2D).

MMP-2 and MMP-9 Activities Are Suppressed in Bsg$^{-/-}$ *Mice*

Bsg is known as an inducer of MMP-2 and MMP-9, and they play a key role in maintaining a balance between ECM deposition and degradation. In addition, the increased synthesis of MMPs has been shown to increase in various kidney diseases.[46,47] Therefore, we next investigated MMP activity in the kidney after UUO. Gelatin zymography demonstrated that the activity of MMP-2 was gradually increased, but was always less in $Bsg^{-/-}$ mice: the difference between the genotypes became apparent 3 days after surgery (Figure 3, A and B). On the other hand, the activation of MMP-9 strikingly increased at 3 days after UUO operation in both genotypes, but to lower extents in $Bsg^{-/-}$ mice at 3 days and 14 days (Figure 3, C and D). Their induction remained higher until 14 days in both groups.

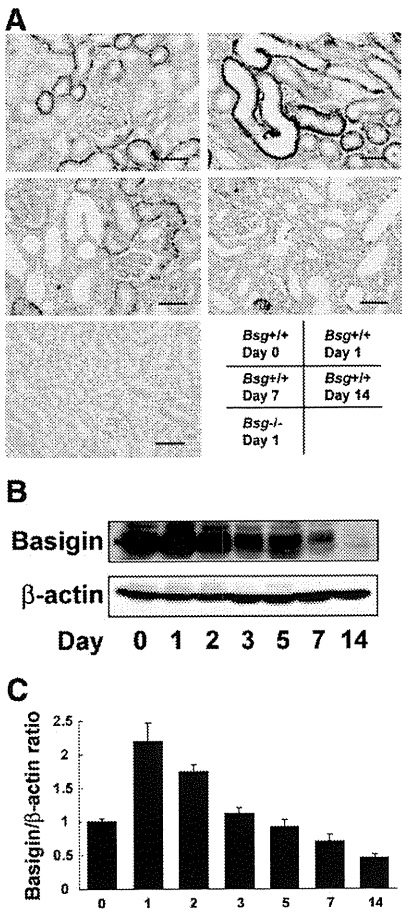

Figure 4. Basigin expression in the UUO model. **A:** Immunohistochemical staining of Bsg in the kidney. Scale bar = 50 μm. **B:** Time course of basigin expression in the UUO model. Bsg protein was determined by Western blotting. **C:** The intensity of Bsg bands was normalized as to β-actin. Data are means ± SD; $^{*}P < 0.05$; $n = 6$.

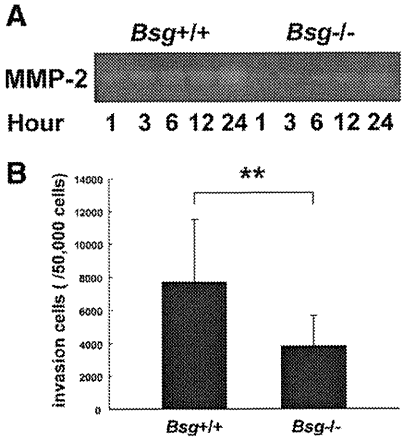

Figure 5. Bsg on TECs contributed to MMP-2 induction and upregulated migration capacity under TGF-β stimuli. **A:** Zymographic analysis indicates MMP-2 production in the culture medium of tubular epithelial cells after TGF-β stimulation. **B:** Migration of tubular epithelial cells was evaluated by cell invasion assay. The number of tubular epithelial cells that had migrated into the lower chamber through basement extract-extracts coated membrane by TGF-β stimulation is indicated. Data are means ± SD; $^{**}P < 0.01$; $n = 30$.

Bsg Expression Is Transiently Upregulated During Acute Phase of Tubulointerstitial Injury

We next examined Bsg expression during the pathogenesis of renal fibrosis. Bsg expression was detected on the basolateral side of the proximal and distal tubules in $Bsg^{+/+}$ mice before UUO operation (Figure 4A), consistent with a previous report.[48] UUO operation transiently and slightly enhanced Bsg expression, reaching the maximum level at day 1 (Figure 4A). However, Bsg expression decreased thereafter, and became very low at day 14 (Figure 4A). Bsg expression was detected in tubular epithelial cells and infiltrating inflammatory cells. The expression reduction was probably attributable to a loss of tubular epithelial cells due to cell death induced by UUO. Western blot data confirmed this observation (Figure 4, B and C). We did not observe any Bsg expression in the kidney of $Bsg^{-/-}$ mice (Figure 4A).

TGF-β Response Is Lower in Primary Bsg$^{-/-}$ *TECs*

Our *in vivo* data showed an apparent association between Bsg and renal fibrosis induced by UUO. To understand the underlying mechanism, we performed *in vitro* experiments. Based on the results shown in Figures 2 and 3, we addressed the effects of Bsg of TECs on MMP-2 production under TGF-β stimulation *in vitro*. When subjected to gelatin zymography, culture media showed that MMP-2 production was indeed induced on TGF-β administration, but the extent of the induction was much lower in $Bsg^{-/-}$ TECs (Figure 5A).

We also examined the invasive capacity of $Bsg^{+/+}$ and $Bsg^{-/-}$ TECs. In the upper chamber, transwell mem-

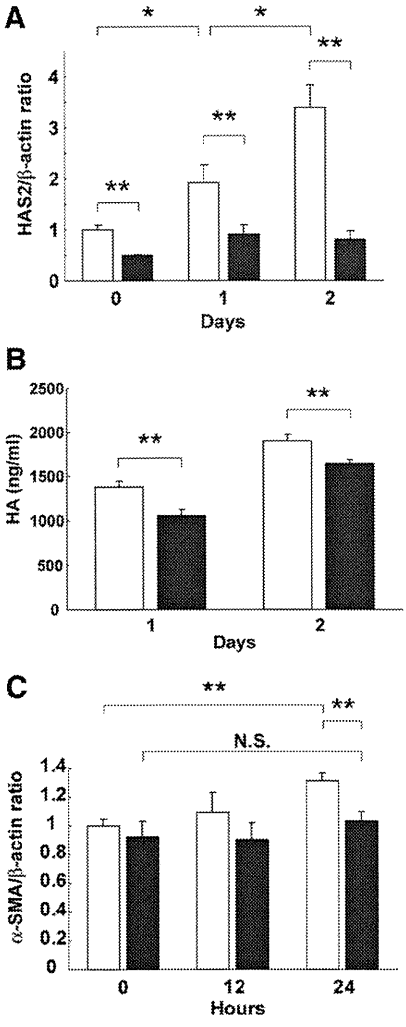

Figure 6. Bsg promoted hyaluronan synthesis and was related to α-SMA induction. **A:** Hyaluronic acid synthase 2 (HAS2) mRNA determined by real-time PCR in MEF under TGF-β stimulation. Each value was standardized by β-actin mRNA content as an internal control. Data are means ± SD; white bar, $Bsg^{+/+}$; black bar, $Bsg^{-/-}$; $^{*}P < 0.05$; $^{**}P < 0.01$; $n = 3$. **B:** Hyaluronan (HA) production in MEF under TGF-β stimulation. White bar, $Bsg^{+/+}$; black bar, $Bsg^{-/-}$; $^{**}P < 0.01$. **C:** α-SMA mRNA determined by real-time PCR in MEF under TGF-β stimuli. Each value was standardized by β-actin mRNA content as an internal control. Data are means ± SD; white bar, $Bsg^{+/+}$; black bar, $Bsg^{-/-}$; $^{**}P < 0.01$; N.S., not significant; $n = 3$.

branes were coated with basement membrane extract, and then TECs were seeded on the membrane. TGF-β was added in the lower chamber. As shown in Figure 5B, $Bsg^{-/-}$ TECs exhibited a lower ability to transmigrate.

Bsg Contributes to Hyaluronan Synthesis on TGF-β Stimulation

Because it has been reported that Bsg promotes hyaluronan production in tumor cells and fibroblasts,[23–25,49] we asked whether or not Bsg deficiency would affect hyaluronan production by MEF. We found that the expression of hyaluronic acid synthase 2, which biosynthesizes hyaluronan, was lower in $Bsg^{-/-}$ MEF even in the steady state (Figure 6A). Furthermore, TGF-β enhanced hyaluronic acid synthase 2 expression in $Bsg^{+/+}$ MEF, but not in $Bsg^{-/-}$ MEF (Figure 6A). We also found the α-SMA mRNA level was elevated 24 hours after TGF-β stimulation in $Bsg^{+/+}$ MEF, but not in $Bsg^{-/-}$ MEF (Figure 6C). This result was in line with recent reports that endogenous hyaluronan promotes α-SMA expression in fibroblast.[10,11]

Discussion

Our *in vivo* data showed that $Bsg^{-/-}$ mice had much less fibrosis, and the difference between the genotypes became apparent 14 days after UUO surgery. MMP-2 and MMP-9 activations were enhanced in both genotypes, but the extent was significantly less in $Bsg^{-/-}$ mice—the difference became apparent as early as 3 days after UUO operation. *In vitro* experiments demonstrated that Bsg on TECs promoted active MMP-2 production in response to TGF-β, and that Bsg on fibroblasts played a critic al role in hyaluronan production in response to TGF-β. Because TGF-β expression was upregulated after UUO to similar extents in $Bsg^{+/+}$ and $Bsg^{-/-}$ mice up to day 7, it is conceivable that the responsiveness to TGF-β is linked to the difference in renal fibrosis in $Bsg^{+/+}$ and $Bsg^{-/-}$ mice. In this context, it is noteworthy that both MMP-2 and MMP-9 are an activator of TGF-β,[4,5] and that Bsg is a strong inducer of MMP family. Thus, there may be a molecular circuit between Bsg, MMPs, and TGF-β (Figure 7). Taken together, our results established that Bsg is an important regulator of renal fibrosis.

UUO is a well-characterized model of renal injury leading to renal fibrosis.[43,50] A number of studies have revealed major pathways leading to the development of renal fibrosis after UUO surgery: the initial event is interstitial infiltration of macrophages that produce cytokines responsible for fibroblast proliferation and activation. After UUO operation, macrophages infiltrate the tubulointerstitial space from blood vessels and become a major source of cytokines, such as TGF-β. Macrophage infiltration was more prominent in $Bsg^{+/+}$ kidneys, and its time course was consistent with the pathogenesis profile of renal fibrosis. It is known that macrophages express Bsg, and that Bsg could be a ligand for E-selectin.[27,34] We also confirmed that Bsg on THP-1, the human monocytic cell line, bound to E-selectin (data not shown). Consider-

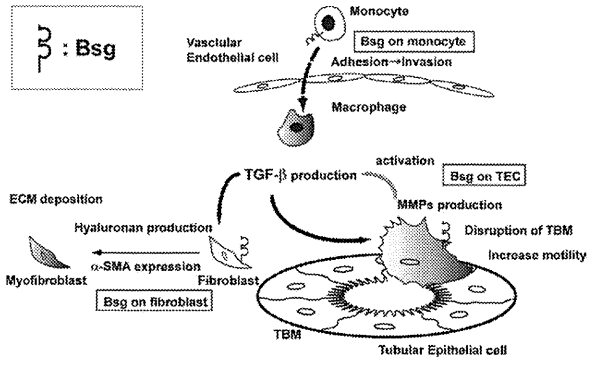

Figure 7. Schematic diagram showing the possible contribution of Bsg to renal fibrosis after UUO.

ing that E-selectin expression was induced to similar degrees in both genotypes, it is likely that the difference in macrophage infiltration between $Bsg^{+/+}$ and $Bsg^{-/-}$ mice is due to the presence of Bsg on macrophages. Indeed, it was reported that mice with triple knockout of E-, P-, and L-selectin show a marked reduction in macrophage infiltration into the obstructed kidney, and are protected from fibrosis in UUO.[51] Thus, macrophage infiltration could be the primary cause of renal fibrosis after UUO, and could cause the difference between $Bsg^{+/+}$ and $Bsg^{-/-}$ mice. In the current study, however, macrophage infiltration began 7 days after surgery, when MMP-2 expression had already been induced (starting from day 3, when TGF-β expression induction was also observed). Therefore, macrophage infiltration cannot fully explain the Bsg involvement with renal fibrosis. Moreover, TGF-β expression was induced to similar extents until 7 days in both genotypes. Our *in vitro* study demonstrated the genotype-dependent responsiveness to TGF-β in TECs and fibroblasts. Together, it is likely that both the Bsg-mediated migration of macrophages and the genotype-dependent responsiveness to TGF-β could be important to the formation of the genotype-dependent difference of renal fibrosis after UUO.

Phenotypic transition of resident renal cells into myofibroblasts is observed in a UUO model. TECs are one of them. Currently, the degree to which this process contributes to kidney fibrosis remains a matter of intense debate.[52,53] Tubular basement membrane regulates numerous cell-matrix interactions that are pivotal to the maintenance of the epithelial phenotype. In the process of renal fibrosis, MMPs are an important factor for the disruption of tubular basement membrane.[54,55] As a result, TECs lose their polarity and acquire contractile motility.[55] Considering that TECs have a TGF-β receptor and produce MMP-2 and MMP-9 on TGF-β stimulation,[56] our data suggest that Bsg on TECs (an inducer of both MMP-2 and MMP-9) is at least partly responsible for disrupting tubular basement membrane and matrix remodeling by MMP induction.

Resident fibroblasts could also be the source of myofibroblasts.[42] Generally, the wound repair process is characterized by the activation of quiescent fibroblasts and their differentiation into myofibroblasts.[30] Hyaluronan promotes α-SMA expression in fibroblasts and orchestrates TGF-β-dependent maintenance of the myofibroblast phenotype.[10,11] Little is known about the precise mechanism underlying how hyaluronan induces α-SMA in fibroblasts, but it is assumed that the hyaluronan macromolecular assembly in the pericellular environment contributes to mediate various signaling.[10] Previous reports and the present study have demonstrated that Bsg promotes hyaluronan production and subsequent α-SMA expression in fibroblasts.[25,49]

In summary, Bsg is a multifunctional molecule engaged in hyaluronan production, MMP production, cell adhesion, and α-SMA induction in renal fibrosis. Intervention targeting Bsg would have multiple effects on the prevention of renal fibrosis.

Acknowledgments

We thank Norihiko Suzuki, Naoko Asano, and Yuriko Sawa for their excellent technical assistance and Hitomi Aoyama for secretarial assistance.

References

1. Schainuck LI, Striker GE, Cutler RE, Benditt EP: Structural-functional correlations in renal disease. II. The correlations. Hum Pathol 1970, 1:631–641
2. Gabbiani G: The myofibroblast in wound healing and fibrocontractive diseases. J Pathol 2003, 200:500–503
3. Mauviel A, Chung KY, Agarwal A, Tamai K, Uitto J: Cell-specific induction of distinct oncogenes of the Jun family is responsible for differential regulation of collagenase gene expression by transforming growth factor-beta in fibroblasts and keratinocytes. J Biol Chem 1996, 271:10917–10923
4. Philipp K, Riedel F, Germann G, Hormann K, Sauerbier M: TGF-beta antisense oligonucleotides reduce mRNA expression of matrix metalloproteinases in cultured wound-healing-related cells. Int J Mol Med 2005, 15:299–303
5. Karsdal MA, Larsen L, Engsig MT, Lou H, Ferreras M, Lochter A, Delaisse JM, Foged NT: Matrix metalloproteinase-dependent activation of latent transforming growth factor-beta controls the conversion of osteoblasts into osteocytes by blocking osteoblast apoptosis. J Biol Chem 2002, 277:44061–44067
6. Yu Q, Stamenkovic I: Cell surface-localized matrix metalloproteinase-9 proteolytically activates TGF-beta and promotes tumor invasion and angiogenesis. Genes Dev 2000, 14:163–176
7. Jenkins RH, Thomas GJ, Williams JD, Steadman R: Myofibroblastic differentiation leads to hyaluronan accumulation through reduced hyaluronan turnover. J Biol Chem 2004, 279:41453–41460
8. Meran S, Thomas D, Stephens P, Martin J, Bowen T, Phillips A, Steadman R: Involvement of hyaluronan in regulation of fibroblast phenotype. J Biol Chem 2007, 282:25687–25697
9. Meran S, Thomas DW, Stephens P, Enoch S, Martin J, Steadman R, Phillips AO: Hyaluronan facilitates transforming growth factor-beta1-mediated fibroblast proliferation. J Biol Chem 2008, 283:6530–6545
10. Webber J, Jenkins RH, Meran S, Phillips A, Steadman R: Modulation of TGFbeta1-dependent myofibroblast differentiation by hyaluronan. Am J Pathol 2009, 175:148–160
11. Webber J, Meran S, Steadman R, Phillips A: Hyaluronan orchestrates transforming growth factor-beta1-dependent maintenance of myofibroblast phenotype. J Biol Chem 2009, 284:9083–9092
12. Biswas C: Tumor cell stimulation of collagenase production by fibroblasts. Biochem Biophys Res Commun 1982, 109:1026–1034
13. Yurchenko V, Constant S, Bukrinsky M: Dealing with the family: cD147 interactions with cyclophilins. Immunology 2006, 117:301–309
14. Biswas C, Zhang Y, DeCastro R, Guo H, Nakamura T, Kataoka H, Nabeshima K: The human tumor cell-derived collagenase stimulatory factor (renamed EMMPRIN) is a member of the immunoglobulin superfamily. Cancer Res 1995, 55:434–439
15. Riethdorf S, Reimers N, Assmann V, Kornfeld JW, Terracciano L, Sauter G, Pantel K: High incidence of EMMPRIN expression in human tumors. Int J Cancer 2006, 119:1800–1810
16. Schneiderhan W, Scheler M, Holzmann KH, Marx M, Gschwend JE, Bucholz M, Gress TM, Seufferlein T, Adler G, Oswald F: CD147 silencing inhibits lactate transport and reduces malignant potential of pancreatic cancer cells in in vivo and in vitro models. Gut 2009, 58:1391–1398
17. Slomiany MG, Grass GD, Robertson AD, Yang XY, Maria BL, Beeson C, Toole BP: Hyaluronan. CD44, and EMMPRIN regulate lactate efflux and membrane localization of monocarboxylate transporters in human breast carcinoma cells. Cancer Res 2009, 69:1293–1301
18. Chen X, Lin J, Kanekura T, Su J, Lin W, Xie H, Wu Y, Li J, Chen M, Chang J: A small interfering CD147-targeting RNA inhibited the proliferation, invasiveness, and metastatic activity of malignant melanoma. Cancer Res 2006, 66:11323–11330
19. Su J, Chen X, Kanekura T: A CD147-targeting siRNA inhibits the proliferation, invasiveness, and VEGF production of human malignant

melanoma cells by down-regulating glycolysis. Cancer Lett 2009, 273:140–147
20. Tang Y, Kesavan P, Nakada MT, Yan L: Tumor-stroma interaction: positive feedback regulation of extracellular matrix metalloproteinase inducer (EMMPRIN) expression and matrix metalloproteinase-dependent generation of soluble EMMPRIN. Mol Cancer Res 2004, 2:73–80
21. Tang Y, Nakada MT, Kesavan P, McCabe F, Millar H, Rafferty P, Bugelski P, Yan L: Extracellular matrix metalloproteinase inducer stimulates tumor angiogenesis by elevating vascular endothelial cell growth factor and matrix metalloproteinases. Cancer Res 2005, 65: 3193–3199
22. Tang Y, Nakada MT, Rafferty P, Laraio J, McCabe FL, Millar H, Cunningham M, Snyder LA, Bugelski P, Yan L: Regulation of vascular endothelial growth factor expression by EMMPRIN via the PI3K-Akt signaling pathway. Mol Cancer Res 2006, 4:371–377
23. Misra S, Ghatak S, Zoltan-Jones A, Toole BP: Regulation of multidrug resistance in cancer cells by hyaluronan. J Biol Chem 2003, 278: 25285–25288
24. Marieb EA, Zoltan-Jones A, Li R, Misra S, Ghatak S, Cao J, Zucker S, Toole BP: Emmprin promotes anchorage-independent growth in human mammary carcinoma cells by stimulating hyaluronan production. Cancer Res 2004, 64:1229–1232
25. Toole BP: Hyaluronan: from extracellular glue to pericellular cue. Nat Rev Cancer 2004, 4:528–539
26. Tang W, Chang SB, Hemler ME: Links between CD147 function, glycosylation, and caveolin-1. Mol Biol Cell 2004, 15:4043–4050
27. Arora K, Gwinn WM, Bower MA, Watson A, Okwumabua I, MacDonald HR, Bukrinsky MI, Constant SL: Extracellular cyclophilins contribute to the regulation of inflammatory responses. J Immunol 2005, 175:517–522
28. Kirk P, Wilson MC, Heddle C, Brown MH, Barclay AN, Halestrap AP: CD147 is tightly associated with lactate transporters MCT1 and MCT4 and facilitates their cell surface expression. EMBO J 2000, 19:3896–3904
29. Philp NJ, Wang D, Yoon H, Hjelmeland LM: Polarized expression of monocarboxylate transporters in human retinal pigment epithelium and ARPE-19 cells. Invest Ophthalmol Vis Sci 2003, 44:1716–1721
30. Huet E, Vallee B, Szul D, Verrecchia F, Mourah S, Jester JV, Hoang-Xuan T, Menashi S, Gabison EE: Extracellular matrix metalloproteinase inducer/CD147 promotes myofibroblast differentiation by inducing alpha-smooth muscle actin expression and collagen gel contraction: implications in tissue remodeling. FASEB J 2008, 22: 1144–1154
31. Igakura T, Kadomatsu K, Kaname T, Muramatsu H, Fan QW, Miyauchi T, Toyama Y, Kuno N, Yuasa S, Takahashi M, Senda T, Taguchi O, Yamamura K, Arimura K, Muramatsu T: A null mutation in basigin, an immunoglobulin superfamily member, indicates its important roles in peri-implantation development and spermatogenesis. Dev Biol 1998, 194:152–165
32. Igakura T, Kadomatsu K, Taguchi O, Muramatsu H, Kaname T, Miyauchi T, Yamamura K, Arimura K, Muramatsu T: Roles of basigin, a member of the immunoglobulin superfamily, in behavior as to an irritating odor, lymphocyte response, and blood-brain barrier. Biochem Biophys Res Commun 1996, 224:33–36
33. Naruhashi K, Kadomatsu K, Igakura T, Fan QW, Kuno N, Muramatsu H, Miyauchi T, Hasegawa T, Itoh A, Muramatsu T, Nabeshima T: Abnormalities of sensory and memory functions in mice lacking Bsg gene. Biochem Biophys Res Commun 1997, 236:733–737
34. Kato N, Yuzawa Y, Kosugi T, Hobo A, Sato W, Miwa Y, Sakamoto K, Matsuo S, Kadomatsu K: The E-selectin ligand basigin/CD147 is responsible for neutrophil recruitment in renal ischemia/reperfusion. J Am Soc Nephrol 2009, 20:1565–1576
35. Chen S, Kadomatsu K, Kondo M, Toyama Y, Toshimori K, Ueno S, Miyake Y, Muramatsu T: Effects of flanking genes on the phenotypes of mice deficient in basigin/CD147. Biochem Biophys Res Commun 2004, 324:147–153
36. Nomura A, Nishikawa K, Yuzawa Y, Okada H, Morgan BP, Piddlesden SJ, Nadai M, Hasegawa T, Matsuo S: Tubulointestinal injury induced in rats by a monoclonal antibody that inhibits function of membrane inhibitor of complement. J Clin Invest 1995, 96:2348–2356
37. Kadomatsu K, Hagihara M, Akhter S, Fan QW, Muramatsu H, Muramatsu T: Midkine induces the transformation of NIH3T3 cells. Br J Cancer 1997, 75:354–359
38. Kosugi T, Yuzawa Y, Sato W, Arata-Kawai H, Suzuki N, Kato N, Matsuo S, Kadomatsu K: Midkine is involved in tubulointerstitial inflammation associated with diabetic nephropathy. Lab Invest 2007, 87:903–913
39. Camussi G, Brentijens JR, Noble B, Kerjaschiki D, Malavasi F, Roholt OA, Farquhar MG, Andres G: Antibody-induced redistribution of Hymann antigen on the surface of cultured glomerular visceral epithelial cells: possible role in the pathogenesis of Hymann glomerulonephritis. J Immunol 1985, 135:2409–2416
40. Tsuboi N, Yoshikai Y, Matsuo S, Kikuchi T, Iwami K, Nagai Y, Takeuchi O, Akira S, Matsuguchi T: Roles of toll-like receptors in C-C chemokine production by renal epithelial cells. J Immunol 2002, 169:2026–2033
41. Nguyen A, Burack WR, Stock JL, Kortum R, Chaika OV, Afkarian M, Muller WJ, Murphy KM, Morrison DK, Lewis RE, McNeish J, Shaw AS: Kinase suppressor of Ras (KSR) is a scaffold which facilitates mitogen-activated protein kinase activation in vivo. Mol Cell Biol 2002, 22:3035–3045
42. Chevalier RL, Forbes MS, Thornhill BA: Ureteral obstruction as a model of renal interstitial fibrosis and obstructive nephropathy. Kidney Int 2009, 75:1145–1152
43. Bascands JL, Schanstra JP: Obstructive nephropathy: insights from genetically engineered animals. Kidney Int 2005, 68:925–937
44. Rouschop KM, Sewnath ME, Claessen N, Roelofs JJ, Hoedemaeker I, van der Neut R, Aten J, Pals ST, Weening JJ, Florquin S: CD44 deficiency increases tubular damage but reduces renal fibrosis in obstructive nephropathy. J Am Soc Nephrol 2004, 15:674–686
45. Wolf G: Renal injury due to renin-angiotensin-aldosterone system activation of the transforming growth factor-beta pathway. Kidney Int 2006, 70:1914–1919
46. Steinmann-Niggli K, Ziswiler R, Kung M, Marti HP: Inhibition of matrix metalloproteinases attenuates anti-Thy1.1 nephritis. J Am Soc Nephrol 1998, 9:397–407
47. Marti HP, McNeil L, Thomas G, Davies M, Lovett DH: Molecular characterization of a low-molecular-mass matrix metalloproteinase secreted by glomerular mesangial cells as PUMP-1. Biochem J 1992, 285(Pt 3):899–905
48. Deora AA, Philp N, Hu J, Bok D, Rodriguez-Boulan E: Mechanisms regulating tissue-specific polarity of monocarboxylate transporters and their chaperone CD147 in kidney and retinal epithelia. Proc Natl Acad Sci U S A 2005, 102:16245–16250
49. Toole BP, Slomiany MG: Hyaluronan. CD44 and Emmprin: partners in cancer cell chemoresistance. Drug Resist Updat 2008, 11:110–121
50. Klahr S, Morrissey J: Obstructive nephropathy and renal fibrosis. Am J Physiol Renal Physiol 2002, 283:F861–875
51. Lange-Sperandio B, Cachat F, Thornhill BA, Chevalier RL: Selectins mediate macrophage infiltration in obstructive nephropathy in newborn mice. Kidney Int 2002, 61:516–524
52. Lin SL, Kisseleva T, Brenner DA, Duffield JS: Pericytes and perivascular fibroblasts are the primary source of collagen-producing cells in obstructive fibrosis of the kidney. Am J Pathol 2008, 173:1617–1627
53. Liu Y: New insights into epithelial-mesenchymal transition in kidney fibrosis. J Am Soc Nephrol 2010, 21:212–222
54. Zavadil J, Bottinger EP: TGF-beta and epithelial-to-mesenchymal transitions. Oncogene 2005, 24:5764–5774
55. Zeisberg M, Maeshima Y, Mosterman B, Kalluri R: Renal fibrosis. Extracellular matrix microenvironment regulates migratory behavior of activated tubular epithelial cells. Am J Pathol 2002, 160:2001–2008
56. Yang J, Liu Y: Dissection of key events in tubular epithelial to myofibroblast transition and its implications in renal interstitial fibrosis. Am J Pathol 2001, 159:1465–1475

Published OnlineFirst February 24, 2011; DOI:10.1158/0008-5472.CAN-10-3524

AACR

Cancer Research

The Neuronal Differentiation Factor NeuroD1 Downregulates the Neuronal Repellent Factor Slit2 Expression and Promotes Cell Motility and Tumor Formation of Neuroblastoma

Peng Huang, Satoshi Kishida, Dongliang Cao, et al.

Cancer Res 2011;71:2938-2948. Published OnlineFirst February 24, 2011.

Updated Version	Access the most recent version of this article at: doi:10.1158/0008-5472.CAN-10-3524
Supplementary Material	Access the most recent supplemental material at: http://cancerres.aacrjournals.org/content/suppl/2011/02/24/0008-5472.CAN-10-3524.DC1.html

Cited Articles	This article cites 29 articles, 13 of which you can access for free at: http://cancerres.aacrjournals.org/content/71/8/2938.full.html#ref-list-1

E-mail alerts	Sign up to receive free email-alerts related to this article or journal.
Reprints and Subscriptions	To order reprints of this article or to subscribe to the journal, contact the AACR Publications Department at pubs@aacr.org.
Permissions	To request permission to re-use all or part of this article, contact the AACR Publications Department at permissions@aacr.org.

Downloaded from cancerres.aacrjournals.org on March 6, 2012
Copyright © 2011 American Association for Cancer Research

Published OnlineFirst February 24, 2011; DOI:10.1158/0008-5472.CAN-10-3524

Cancer Research

The Neuronal Differentiation Factor NeuroD1 Downregulates the Neuronal Repellent Factor Slit2 Expression and Promotes Cell Motility and Tumor Formation of Neuroblastoma

Peng Huang[1], Satoshi Kishida[1], Dongliang Cao[1], Yuko Murakami-Tonami[1], Ping Mu[1], Masato Nakaguro[1], Naoshi Koide[1], Ichiro Takeuchi[2], Akira Onishi[3], and Kenji Kadomatsu[1]

Abstract

The basic helix-loop-helix transcription factor NeuroD1 has been implicated in the neurogenesis and early differentiation of pancreatic endocrine cells. However, its function in relation to cancer has been poorly examined. In this study, we found that NeuroD1 is involved in the tumorigenesis of neuroblastoma. NeuroD1 was strongly expressed in a hyperplastic region comprising neuroblasts in the celiac sympathetic ganglion of 2-week-old *MYCN* transgenic (Tg) mice and was consistently expressed in the subsequently generated neuroblastoma tissue. NeuroD1 knockdown by short hairpin RNA (shRNA) resulted in motility inhibition of the human neuroblastoma cell lines, and this effect was reversed by shRNA-resistant NeuroD1. The motility inhibition by NeuroD1 knockdown was associated with induction of Slit2 expression, and knockdown of Slit2 could restore cell motility. Consistent with this finding, shRNA-resistant NeuroD1 suppressed Slit2 expression. NeuroD1 directly bound to the first and second E-box of the Slit2 promoter region. Moreover, we found that the growth of tumor spheres, established from neuroblastoma cell lines in *MYCN* Tg mice, was suppressed by NeuroD1 suppression. The functions identified for NeuroD1 in cell motility and tumor sphere growth may suggest a link between NeuroD1 and the tumorigenesis of neuroblastoma. Indeed, tumor formation of tumor sphere–derived cells was significantly suppressed by NeuroD1 knockdown. These data are relevant to the clinical features of human neuroblastoma: high NeuroD1 expression was closely associated with poor prognosis. Our findings establish the critical role of the neuronal differentiation factor NeuroD1 in neuroblastoma as well as its functional relationship with the neuronal repellent factor Slit2. *Cancer Res; 71(8); 2938–48. ©2011 AACR.*

Introduction

NeuroD1 is a basic helix-loop-helix (bHLH) transcription factor. *NeuroD1*-deficient mice die as a consequence of severe hyperglycemia within 5 days of birth (1). This is attributed to differentiation deficit and death of β cells in the pancreas during embryogenesis (1). In addition, NeuroD1 is involved in neurogenesis. It can convert embryonic epidermal cells into fully differentiated neurons in *Xenopus* and promotes premature cell-cycle exit and differentiation of neural precursor cells (2). By crossing *NeuroD1*-deficient mice with either transgenic mice expressing NeuroD1 in β cells or (mammalian atonal homolog) *MATH*-deficient mice, Miyata and colleagues as well as Schwab and colleagues demonstrated that NeuroD1 deletion in the central nervous system leads to depletion of the cerebellar granule cells and loss of the dentate gyrus in the hippocampus (3, 4). Furthermore, NeuroD1 is involved in the differentiation of peripheral neurons. Thus, *NeuroD1*-deficient mice exhibit neuronal cell loss in the inner ear (5, 6). In the retina of *NeuroD1*-deficient mice, amacrine cell differentiation is perturbed and the number of bipolar interneurons decreases (7). Furthermore, it has recently been reported that NeuroD1 plays an essential role in the maintenance of neural precursor cells in adult neurogenesis: inducible stem cell–specific deletion of NeuroD1 causes fewer newborn neurons in the hippocampus and the olfactory bulb (8, 9).

Neuroblastoma (NB) is the most common extracranial pediatric solid tumor and is derived from the sympathetic neuron lineage of neural crest cells (10). A hierarchical expression of regulatory molecules, such as Sox2, BMP, Mash1, Phox2B, and Hand2, determines the fate of neural crest cells and their further differentiation to form sympathetic neurons (11). The molecular mechanism of the normal development of sympathetic neurons may influence the biology of NB. For

Authors' Affiliations: [1]Department of Biochemistry, Nagoya University Graduate School of Medicine; [2]Department of Computer Science/Scientific and Engineering Simulation, Nagoya Institute of Technology, Nagoya; and [3]Transgenic Animal Research Center, National Institute of Agrobiological Sciences, Tsukuba, Ibaraki, Japan

Note: Supplementary data for this article are available at Cancer Research Online (http://cancerres.aacrjournals.org/).

Corresponding Author: Kenji Kadomatsu, Department of Biochemistry, Nagoya University Graduate School of Medicine, 65 Tsurumai-cho, Showa-ku, Nagoya 466-8550, Japan. Phone: 81-52-744-2059; Fax: 81-52-744-2065; E-mail: kkadoma@med.nagoya-u.ac.jp

doi: 10.1158/0008-5472.CAN-10-3524

©2011 American Association for Cancer Research.

American Association for Cancer Research

Downloaded from cancerres.aacrjournals.org on March 6, 2012
Copyright © 2011 American Association for Cancer Research

Published OnlineFirst February 24, 2011; DOI:10.1158/0008-5472.CAN-10-3524

example, the homeodomain DNA-binding transcription factor Phox2B is mutated in familial and sporadic forms of NB (12). Phox2B mutations predispose to NB by promoting the proliferation and dedifferentiation of cells in the sympathoadrenergic lineage (13). Phox2B induction in a NB cell line downregulates expression of the homeobox protein Msx1, whereas Msx1 upregulates expression of Notch3 and Hey1 and downregulates NeuroD1 expression (14). The bHLH transcription factor Hand2, the proto-oncogene *MYCN*, and tyrosine hydroxylase, which is essential for catecholamine metabolism, are expressed in proliferating precursors of sympathetic neurons (15). *MYCN* gene amplification is often observed in NB, and it is the strongest prognostic factor of NB (16). Furthermore, the bHLH transcription factor *Mash1*-deficient mice lose sympathetic neurons (17). Mash1 is expressed in multipotent neuron progenitors immediately after expression of neural stem cells during postnatal hippocampus granule neurogenesis, whereas NeuroD1 is expressed in more differentiated progenitors (18). Mash1 is expressed mostly in poorly differentiated neuroendocrine carcinoma, whereas NeuroD1 is expressed in well-differentiated neuroendocrine carcinoma (19).

Weiss and colleagues generated *MYCN* transgenic (Tg) mice, in which MYCN expression is targeted to the sympathetic neuron lineage by the rat tyrosine hydroxylase (20). These mice develop NB in the celiac sympathetic ganglion, which has histology indistinguishable from that of human NB (20). In particular, hemizygous mice develop tumors with a stepwise increase of the frequency of *MYCN* amplification (21). Therefore, this model mimics human NB development. Moreover, this model demonstrates a marked increase of neuroblast hyperplasia at approximately 2 weeks after birth that is hypothesized to represent a precancerous lesion (21).

In spite of the accumulating evidence showing the critical roles of NeuroD1 in neurogenesis, its involvement in cancer development has not been fully explored. As NB tumorigenesis is closely related to the normal development of the sympathetic neuron lineage, we hypothesized that NeuroD1 could be an important regulator of NB. To examine this hypothesis, we used *MYCN* hemizygous mice and found that NeuroD1 plays a critical role in NB tumorigenesis.

Materials and Methods

RT-PCR

Thermal conditions for PCR included 28–35 cycles of denaturing at 94°C for 30 seconds, annealing at 55–56°C for 30 seconds, and elongation at 72°C for 30 seconds. The primers used and the expected product sizes are listed in Supplementary Table SI. Detection of NeuroD1 and Slit2 was performed by using the TaqMan Gene Expression Assays kit (Applied Biosystems) according to the manufacturer's instructions. The assay ID for NeuroD1 is Hs00159598_m1 and that for Slit2 is Hs00191193_m1.

RNA interference

Nontargeting short hairpin RNA (shRNA; Sigma) and specific shRNA for human NeuroD1 (Sigma), mouse NeuroD1 (Open Biosystems), and human Slit2 (Open Biosystems) were used. The shRNA sequences are listed in Supplementary Table SII. Together with the lentivirus packaging plasmids psPAX2 (Addgene plasmid 12260) and pMD2.G (Addgene plasmid 12259), all plasmids were cotransfected into HEK293T cells to produce infectious virus particles. The titer was evaluated by using a QuickTiter Lentivirus Titer kit (Cell Biolabs). Approximately 2.5×10^9/mL virus particles were obtained. NB cells were infected in the presence of 8 μg/mL polybrene (Sigma). For the infection of tumor sphere cells, virus particles were concentrated by PEG-it Virus Precipitation Solution (System Biosciences) and suspended in a sphere growth medium without polybrene.

Plasmids

A human NeuroD1 cDNA clone was amplified from human HEK293 cell cDNA with attB-flanked primers. For shRNA-resistant expression constructs, the shRNA-targeting site on the cDNA was mutated at 6 nucleotides without affecting the amino acid sequence. Thereafter, following the instructions of Invitrogen Gateway Technology and using the ClonaseII Kit, the mutated NeuroD1 cDNA was inserted into the gateway destination vector CSII-CMV-RfA-IRES2-Venus (RIKEN BioResource Center, Ibaraki, Japan), which is a lentivirus-based cDNA over-expression vector. CSII-CMV-Venus (RIKEN) was used as the negative control.

Histochemistry and Western blot analysis

Tissues were fixed in 4% paraformaldehyde, dehydrated, and embedded in paraffin according to the standard procedure. Then, 5-μm sections were stained with hematoxylin and eosin stain or incubated with anti-NeuroD1 polyclonal antibody (Cell Signaling Technology), which was diluted at a concentration of 1:50 in 3% normal goat serum for 2 hours at room temperature, and then incubated with biotin goat anti-rabbit secondary antibody (1:50; BD Pharmingen) for 30 minutes at room temperature. For Western blot analysis, anti-NeuroD1 (1:500; Santa Cruz Biotechnology), anti-Slit2 (1:500; Millipore), and anti-β-actin (1:10,000; Sigma) antibodies were used.

ChIP assay

SH-SY5Y cells were cross-linked by 1% formaldehyde, and the reaction was quenched with 0.125 mol/L glycine. Cells were harvested by using PBS containing phenylmethylsulfonylfluoride (PMSF) followed by homogenization with hypotonic buffer. Then, DNA was digested to 150 to 900-bp fragments with micrococcal nuclease (New England Biolabs). The pellet obtained was resuspended in 300 μL of lysis buffer containing propidium iodide and sonicated. The lysates were centrifuged, and the supernatants obtained were diluted with dilution buffer. Furthermore, these lysates were incubated with control Immunoglobulin G1 (IgG1) antibody (R&D Systems) or anti-NeuroD1 (Santa Cruz Biotechnology) accompanied by rotation for 4 hours at 4°C this was followed by the addition of 15 μL of protein G Sepharose (GE Healthcare) and rotation for 1 hour at 4°C. The precipitants obtained were washed, eluted with elution buffer, and subjected to PCR. The

Downloaded from cancerres.aacrjournals.org on March 6, 2012
Copyright © 2011 American Association for Cancer Research

Published OnlineFirst February 24, 2011; DOI:10.1158/0008-5472.CAN-10-3524

chromatin immunoprecipitation (ChIP) primer sequences are listed in Supplementary Table SI.

Wound-healing assay and Boyden chamber assay

A total of 2×10^5 cells were plated in a 6-well plate, and, 24 hours later, infected with virus. For the wound-healing assay, another 48 hours later, a scratch on the confluent monolayers of cells was made using a plastic pipette tip. The cell-migration area was calculated by using Metamorph 6.1 software (Molecular Devices), and it was represented as the change in length (μm). For the Boyden chamber assay, cells were harvested 48 hours after virus infection and counted. Transwell plates (pore size: 8 μm; Corning) were used. The undersurface of the chamber was coated with 10 μg/mL collagen I (Upstate Biotechnology). Virus-infected cells were seeded in the upper chamber (4×10^4 per well) with 1% bovine serum albumin. Thereafter, 10% FBS was added to the lower chamber. Cells were allowed to migrate for 6 hours. Nonmigrated cells in the upper chamber were removed by using a swab. Migrated cells attached to the lower side of chamber were stained with 4′,6-diamidino-2-phenylindole and counted in 4 randomly selected fields. Then, 4 fields at 100 times the magnitude per sample were selected. The experiment was performed twice, with each sample in triplicate.

Animals

The *MYCN* Tg mice (20) were maintained in our animal facility, where they were housed under a controlled environment and provided with standard nourishment and water. Tumor tissues from hemizygous *MYCN* Tg mice were dissected, minced, and then inoculated subcutaneously into 1-month-old 129/SVJ wild-type (WT) mice (the mouse strain of *MYCN* Tg mice). After approximately 15 such serial passages, a more invasive tumor was obtained. This constituted our allograft model in the present study. This study was approved by the Animal Care and Use Committee of Nagoya University Graduate School of Medicine, Nagoya, Japan.

Tumor sphere culture and allograft tumorigenesis

A 0.5-cm^3 tumor tissue was dissected and washed several times with Hanks' balanced salt solution (HBSS). After thorough mincing, cells were digested with 0.25% trypsin (5 mL) at 37°C for 10 minutes. The same volume of trypsin inhibitor (Sigma) was used to stop the digestion. After centrifuging and washing with HBSS, the tissue pellet was mixed with 5 mL HBSS and allowed to react for 10 minutes. Thereafter, the supernatant was carefully transferred to a new tube and centrifuged. The cell pellet was suspended in a growth medium for stem cells [Dulbecco's modified Eagle Medium (DMEM):F12K 1:1, epidermal growth factor 10 ng/mL, basic fibroblast growth factor 15 ng/mL) and seeded onto a 10-cm petri dish. The medium was changed 24 hours later to remove dead cells. Approximately 2 days later, tumor spheres were recognized. These tumor spheres were digested with trypsin and broken down into single cells and were passed through fresh culture every 3–4 days. For the allograft tumorigenesis experiment, 1×10^4 shRNA-treated cells mixed with 30% Matrigel (BD Biosciences) were subcutaneously inoculated into 1-month-old 129/SVJ WT mice. Eighteen days later, the tumors were dissected and weighed.

Cell culture

SH-SY5Y cells were obtained from the American Type Culture Collection. IMR32 cells were procured from RIKEN. We monitored the morphology of these cells by microscopic examination and confirmed that their morphology was the same as that of the original cells. In addition to cell growth and morphology, we also confirmed that IMR32 cells strongly expressed *MYCN* whereas SH-SY5Y cells did not. No further validation was performed during these experiments. Stable NeuroD1-knockdown SH-SY5Y cells were maintained in DMEM with 10% FBS and 1 μg/mL puromycin (InvivoGen).

Data analysis

Results are expressed as the mean ± SD. Statistical significance was evaluated by Student's t test.

Results

NeuroD1 is expressed in the hyperplastic region of sympathetic ganglions

We examined the NeuroD1 expression profile during the tumorigenesis of NB in *MYCN* Tg mice. As previously reported (21), we found that neuroblast hyperplasia occurred in the celiac sympathetic ganglions approximately 2 weeks after birth in *MYCN* Tg mice but not in WT mice [Fig. 1A (a and b)]. There were several loci of neuroblast hyperplasia in a ganglion [Fig. 1A (b)]. Because the incidence of hyperplasia correlates with the incidence of tumor formation in *MYCN* Tg mice, neuroblast hyperplasia is considered to be the precancerous status of NB (21). We found that ganglion cells of WT mice, at 2 weeks after birth, showed only low-level expression of NeuroD1 [Fig. 1A (c)]. Surprisingly, NeuroD1 was strongly expressed in the hyperplastic loci in *MYCN* Tg mice [Fig. 1A (d), arrowheads], whereas only low-level expression of NeuroD1 was detected in the surrounding ganglion cells [Fig. 1A (d)]. The expression was strong in the majority of hyperplastic cells but not necessarily in all cells [Fig. 1A (d)]. We confirmed the presence of NeuroD1 mRNA expression in the hyperplastic ganglions of *MYCN* Tg mice by using RT-PCR, but the expression in WT ganglion was below the detection threshold (Fig. 1B). Furthermore, we found that there was continued NeuroD1 expression in advanced cancerous tissues of NB derived from *MYCN* Tg mice (Fig. 1C). Interestingly, NeuroD1 expression was not homogenous, but rather a portion of the total cancer cells strongly expressed it (Fig. 1C).

Hyperplasia in WT mice usually regresses approximately 2 weeks after birth (21). Therefore, we subsequently questioned whether hyperplasia in WT mice at an early age could also express NeuroD1. We found neuroblast hyperplastic regions in the celiac sympathetic ganglions at day 0 after birth in both WT and *MYCN* Tg mice, as previously reported [Fig. 1D (a and b); ref. 21]. While there was low-level expression of NeuroD1 in immature ganglion cells in both genotypes [Fig. 1D (a and b, white arrowheads], NeuroD1 expression was barely detectable in neuroblast hyperplastic regions at this age

Downloaded from cancerres.aacrjournals.org on March 6, 2012
Copyright © 2011 American Association for Cancer Research